INVESTIGATIONS OF THE MECHANISM OF DNA CLEAVAGE USING RUTHENIUM POLYPYRIDYL COMPLEXES

by

FIONA ONGERI

Presented to the Faculty of the Graduate School of

The University of Texas at Arlington in Partial Fulfillment

of the Requirements for the Degree of

MASTER OF SCIENCE IN CHEMISTRY

THE UNIVERSITY OF TEXAS AT ARLINGTON

May 2007

ACKNOWLEDGEMENTS

I would like to express my deep thanks to my research advisor, Prof. Frederick MacDonnell for giving me the great opportunity to study in his laboratory and for all his guidance and support throughout my studies. I am very grateful for all the advice and patience he has had with me. He has been an inspiring leader and has taught me to never give up even though circumstances may seem dire. Once again, I thank him for his understanding, patience, and sense of humor.

I would also like to thank my thesis committee, Dr. Subhrangsu Mandal and Dr. Jongyun Heo who very supportive and were always ready to help me with any questions that I had. I gratefully thank to them for their efforts. I would also like to say a huge thank you to Dr Norma de Tacconi for all of her help and guidance.

Also, I would like to take this opportunity to express gratitude to all my colleagues: Abhishek (Team Skippy!), Tamara, Cale, Arthi, Kelly, Shreeyyukta, Manas, Nancy and Gatachew. Specials thank also to the Chemistry Department staff. I would also like to say a special thank you to my family, Nyagaka, Carol, Sylvia, and friends Chammi, Risper, Sophie, Lilly, Martha, Getrude, Maya, Dennis, Heb, Rhoda, Tankiso and Derrick for all their support and prayers.

I am also forever grateful to my parents; Prof. Samson Ongeri and Elizabeth Ongeri for their never ending love, support and prayers.

Finally, I would also like to thank God for giving me the opportunity and the strength to go through this.

April 15, 2007

ABSTRACT

INVESTIGATIONS OF THE MECHANISM OF DNA CLEAVAGE

USING RUTHENIUM POLYPYRIDYL COMPLEXES

Publication No. _____

Fiona Ongeri, M.S.

The University of Texas at Arlington, 2007

Supervising Professor: Prof. Frederick MacDonnell

We have synthesized a ruthenium complex, $[(phen)_2Ru(tatpp)Ru(phen)_2]^{4+}$ ($\mathbf{P^{4+}}$), which has been shown to undergo various redox and protonation steps to form different species that can be monitored by UV-Vis spectroscopy. In Chapter 2, the photochemistry of $\mathbf{P^{4+}}$ in the presence and absence of DNA was studied. It was hypothesized that the lifetime of the excited state ($t_{1/2}$) of $\mathbf{P^{4+}}$, **P*,** would be extended in the presence of DNA. However, studies conducted showed that the lifetime of **P*** was diminished in the presence of DNA as compared to $\mathbf{P^{4+}}$ alone.

Experiments have also shown that $\mathbf{P^{4+}}$ is capable of damaging DNA both in the presence and absence of oxygen. This damage is potentiated under anaerobic

conditions. In Chapter 3, we uncovered the chemical species responsible for damaging plasmid DNA as the doubly reduced, doubly protonted $\mathbf{H_2P^{4+}}$ species and a carbon-based radical species.

TABLE OF CONTENTS

LIST OF ILLUSTRATIONS

LIST OF SCHEMES

CHAPTER 1

INTRODUCTION

1.1 Metals used as DNA cleaving agents

According to the American Cancer Society, cancer is the second leading cause of death in the United States. For this reason, over the past 40 years, there has been a vast interest in development of efficient anticancer drugs that possess minimal side effects. Cancer is a class of diseases in which there is uncontrolled cell division. Malignant tumor cells can spread directly into adjacent tissue or indirectly by metatasis. Once these cancerous cells spread, they are difficult to treat.

Transition metal complexes have been of interest in the field of cancer research. This is mainly due to the fact that they exhibit unique spectral and electrochemical signatures, as well as the ability of their ligands to be modulated to DNA binding and cleaving abilities. The most popular metal analogues on the market today are those that contain Platinum and Ruthenium. Other metal analogues containing Copper, Iron and Chromium are still under development.

1.2 Platinum complexes

To date, cisplatin (*cis*-diamminedichloro-platinum (II)) is one of the most successful anticancer drugs in the market (Figure 1.1). Cisplatin as an anticancer drug, was first in the 1960's by Rosenberg and co-workers.[1] Cisplatin is one of the most

commonly used cytotoxic agents in the treatment solid malignant tumors such as those found in the head and neck, lungs, ovary, bladder and testicles.[2,3] Although treatment with cisplatin is often effective, serious side-effects such as nausea, nephrotoxicity, neurotoxicity and ototoxicity occur often.[4] In addition, cisplatin, which is administered intravenously, has limited solubility in aqueous solution.[5] This has lead to intensive efforts in developing newer platinum drugs that will show similar efficiency of cisplatin but exhibit less toxicity.

The first successful development of a cisplatin analogue was carboplatin (*cis*-diammine(1,1-cyclobutanedicarboxylato)platinum (II)) (Figure 1.1). Cisplatin and carboplatin have similar structures except for the fact that the unidentate chloride ligands found in cisplatin are replaced by a chelating cyclobutanedicarboxylate. This carboxylate moiety helps in the increasing the drugs solubility in water.[6] Even though carboplatin has been found to be less potent than cisplatin, it has less cytotoxic effects while still showing a similar spectrum of activity.

Oxaliplatin, (*trans*-1,2-diamminocyclohexaneoxalaplatinum (II)) is another analogue of cisplatin (Figure 1.1). This compound lacks the cross resistance found in some cisplatin resistant models due to the 1,2-diaminocyclobutane ligand (DACH).[5] Oxaliplatin has received clinical approval in France for the treatment of colorectal cancer.[7,8]

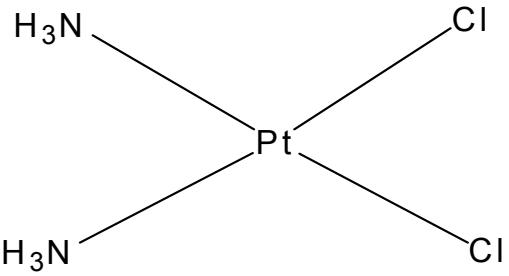

Cisplatin

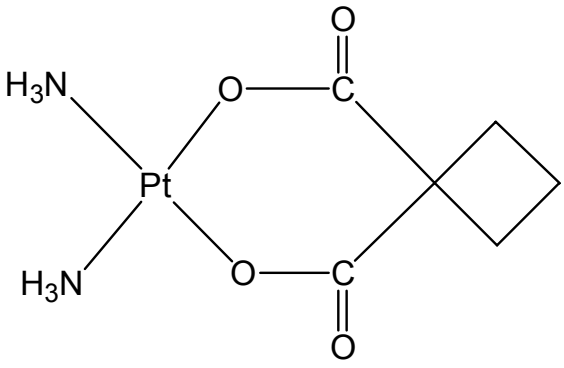

Carboplatin

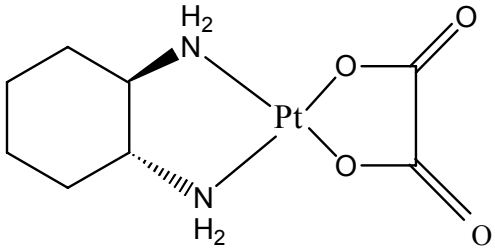

Oxaliplatin

Figure 1.1 Platinum based anticancer drugs.

1.3 Ruthenium complexes

Over the past several years, the interaction of polypyridyl Ru (II) complexes with DNA has been the focus of several research works. Ru (II) polypyridyl complexes are of particular interest due to a combination of stability, ease of construction, chirality

and opto-electronic properties.[9] Barton and coworkers were one of the first groups to explore the interactions of positively charged transition metal complexes with DNA and note their use under physiological conditions.[10] Keppler and other researchers observed that certain Ru (II) complexes exhibit high anti-tumor activity.[11]

1.3.1 Binding studies of some ruthenium complexes

Ruthenium (II) polypydiryl classes of metallointercalators have received particular attention due to their luminescence characteristics and strong DNA binding affinities. The binding of Ru (II) complexes to DNA is sensitive to shape, size, chirality and hydrophobic character.[9]

The binding studies of ruthenium based monomers have been extensively studied. One of the earliest binding studies for a ruthenium monomer was conducted on enatiomeric $[Ru(phen)_3]^{2+}$ (Figure 1.2) and was shown to have a binding constant of 10^3 M^{-1}.[12,13] It has also been proposed that the cationic $[Ru(phen)_3]^{2+}$ complexes can bind to DNA *via* three non-covalent modes namely; electrostatically, hydrophobically binding to the minor groove or by partial intercalation of the phenanthroline ligand into DNA.[9] However, works by Ericksson et al. proposed that both the Δ and the Λ $[Ru(phen)_3]^{2+}$ bind to DNA only *via* intercalative fashion in the minor groove.[14]

The binding studies for $[Ru(bpy)_2dppz]^{2+}$ with DNA have been conducted showing that extension of the bridging ligand increases the binding constant to ~10^6 M^{-1}. These complexes have expansive aromatic surface areas that show high affinity for DNA.[15] Interestingly, these complexes do not luminescence in aqueous solution, however when bound to DNA, luminescence brightly. On the basis of NMR studies

conducted by Dupureur and Barton, these complexes have been found to intercalate into the major groove resulting in DNA damage.[16,17] The binding geometry of these complexes has yet to be firmly defined.

Further studies conducted by Lincoln and co-workers on $[Ru_2(phen)_4(bis\text{-}dppz)]^{4+}$ have found that the addition of a second ruthenium center further increases the interaction between the metal compound and DNA hence the binding constant increases to $\sim 10^8\ M^{-1}$.

Overall Ru (II) complexes have been shown to be good DNA-adducts that can be used as potential anticancer chemotherapeutic agents.

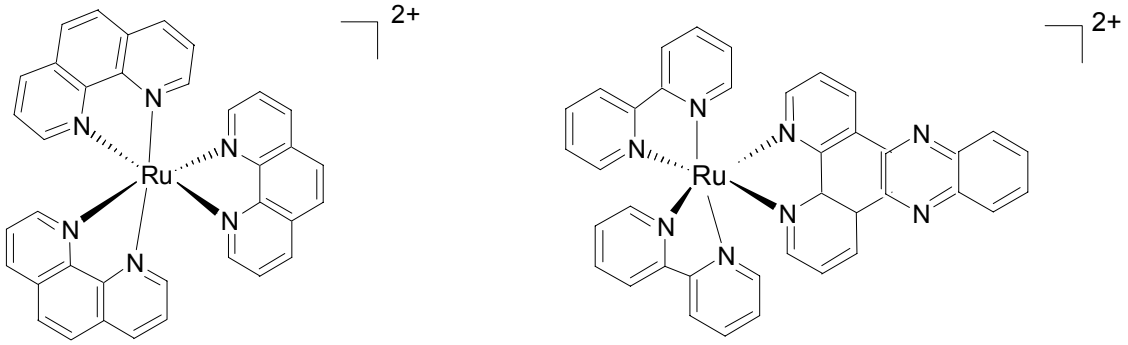

$Ru(phen)_3$ **$Ru(bpy)_2dppz$**

Figure 1.2 Structures of cationic ruthenium complexes, $[Ru(phen)_3]^{2+}$ (phen = 1,10-phenathroline) and $[Ru(bpy)_2dppz]^{2+}$ (bpy = 2,2' bipyridyl dipyrido [3,2-*a*:2',3'-*c*] phenazine.

1.3.2 Ruthenium based anticancer agents

Among all the ruthenium-based anticancer agents, Ruthenium-DMSO complexes are believed to show the greatest potential as anticancer agents due to their selectivity for solid tumor metastases and low toxicity *in vivo*.[18] Antimetastatic activity of Ruthenium-DMSO complexes was first discovered in the early 1980's with *cis* and *trans* $[RuCl_2(DMSO)_4]$. However, these complexes showed poor solubility. This led to further investigations of ruthenium complexes that would exhibit greater solubility. Keppler et. al. synthesized $ImH[RuCl_4Im_2]$, a new series of Ru (III) derivatives containing heterocyclic ligands. These compounds were shown to have anticancer activity in model colon-rectal tumors in carcinogen treated rats.[11] Based on these results, Sava investigated two Ru (III) derivatives namely, Na[*trans*-$RuCl_4$(DMSO)Im] NAMI (Figure 1.3) and *mer*-$RuCl_3(DMSO)_2Im$. These complexes were tested against various solid metastasizing tumors in mice and were found to be active in Lewis lung carcinomas, B16 melanomas and MCa mammary carcinomas. In addition, NAMI has also been shown not to induce any liver, kidney or lung toxicity. [19]

Replacement of Na^+ with ImH^+ yielded $[H_2Im]$[*trans*-$RuCl_4$(DMSO)Im], NAMI-A (Figure 1.3). NAMI-A is almost identical to NAMI as far as anti-matastatic activity but is more stable in air and has no free sulfoxide in crystalline structure. NAMI-A has successfully completed Phase I clinical trials.

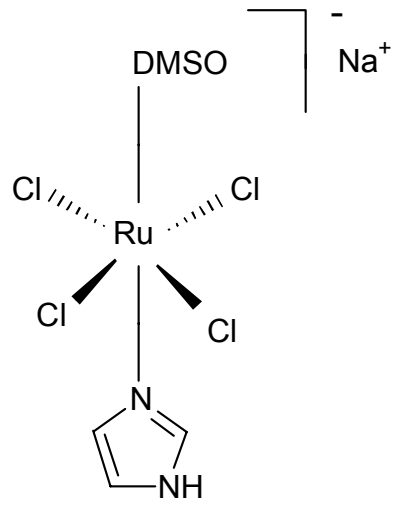

(Na)[*trans*-[$RuCl_4$(DMSO)(Im)

NAMI

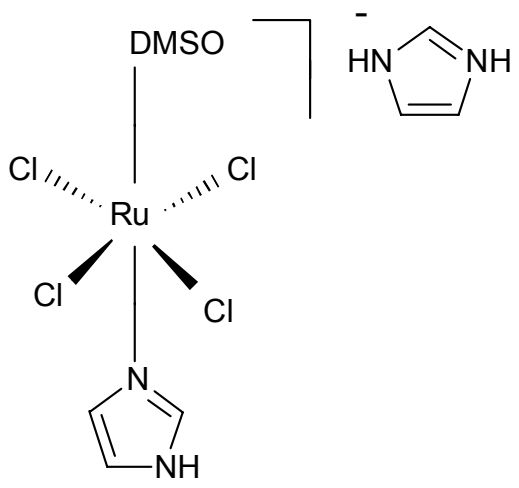

(ImH)[*trans*-[$RuCl_4$(DMSO)(Im)

NAMI-A

Figure 1.3 Potential Ruthenium complexes used to treat tumor metastases.

It is thought that the architecture and mechanism of the NAMI-A DNA adduct formation may differ from that of cisplatin. NAMI-A complexes are known to alter the ratio between certain matrix metalloproteins (e.g. MMP-2) and their inhibitors, TIMP's (e.g. TIMP-2) thereby increasing the extracellular matrix components in the tissue parenchyma and surrounding tumor blood vessels, which prevents the spread of the tumor cells into surrounding tissue. However, the exact mechanism as to how this process occurs has yet to be fully established. [20-22]

1.4 Mechanisms of DNA cleavage

Most prospective metal-based drugs on the market require dioxygen to bring about DNA damage. Even fewer have been shown to induce damage *via* carbon centered radicals. We will take brief look as to how DNA damage is brought about *via* these two pathways.

1.4.1 Reactive oxygen species (ROS)

McCord and Fridovich were the first to discover that the enzyme superoxide dismutase is able to dismutate superoxide anion to form oxygen and hydrogen peroxide.[23] These ROS have been found to interact directly with DNA or DNA components *via* singlet oxygen species ($O_2^{\bullet -}$) and hydroxide radicals ($^{\bullet}OH$). Under aerobic conditions, react with oxygen to produce $O_2^{\bullet -}$ (E = ~0.9 V vs. NHE).[24] However, several works in literature have shown that $O_2^{\bullet -}$ radicals cannot induce DNA damage.[25] These $O_2^{\bullet -}$ can react with H^+ to generate H_2O_2 which in turn can react with more $O_2^{\bullet -}$ to generate more $^{\bullet}OH$ *via* Harber-Weiss reactions. The redox potential for $^{\bullet}OH$ radicals is E = ~2.4 V vs. NHE. Since the redox potential for $^{\bullet}OH$ is high, $^{\bullet}OH$ can oxidize DNA, resulting in DNA damage.

ROS induce oxidative stress. *In vivo*, radicals are thought to be produced *via* two main pathways. The first is *via* the exposure of living organisms to ionizing radiation (γ radiolysis) leading to the hemolytic fission of oxygen-hydrogen bonds in water thereby producing an $^{\bullet}OH$. The second way is through the generation of $^{\bullet}OH$ through Fenton reactions (Figure 1.4). These reactions usually involve a ferrous ion

which acts as a catalyst in the presence of hydrogen peroxide. The hydrogen peroxide is broken down into a hydroxide ion and a hydroxyl free radical.

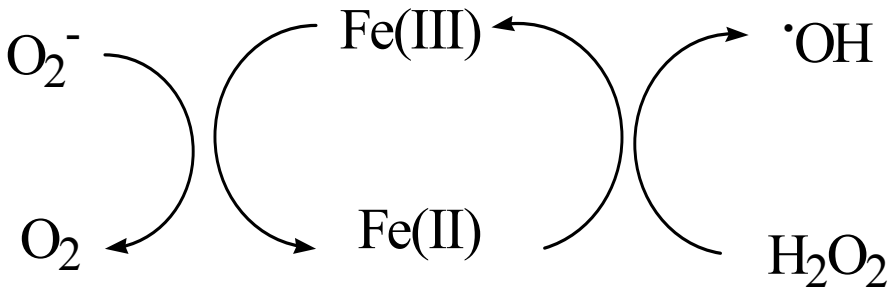

Figure 1.4 Schematic diagram showing iron conversion to hydroxyl radicals.

It has been shown that DNA ·OH radicals induce DNA damage *via* hydrogen abstraction from the sugar moiety hence forming sugar radicals.[26] Schraufstatter and coworkers were the first to show that exposure of H_2O_2 to P388 D1 cells resulted in an increase in 8-hydroxyguanine (8-OH-Gua).[27] Later, Floyd et al. was able to prove that the major product formed by ·OH DNA damage was 8-OH-Gua suggesting that ·OH radicals are involved in the attack of purine bases.[28]

Three major intermediates that result from ·OH radical attack has been identified (Figure 1.5). The chemical fates of these intermediates have been extensively studied. Adduct **1** and **2** revert back to guanine by gaining an electron via thiols generated in the cells. Adduct **3** (8-OH-Gua) leads to the formation of 7,8-dihydro-8-oxoguanine or can gain an electron and a proton forming 2,6-diamino-5-formamido-4-hydroxypyrimidine (FAPy-G) which eventually lead to DNA damage.[29-31]

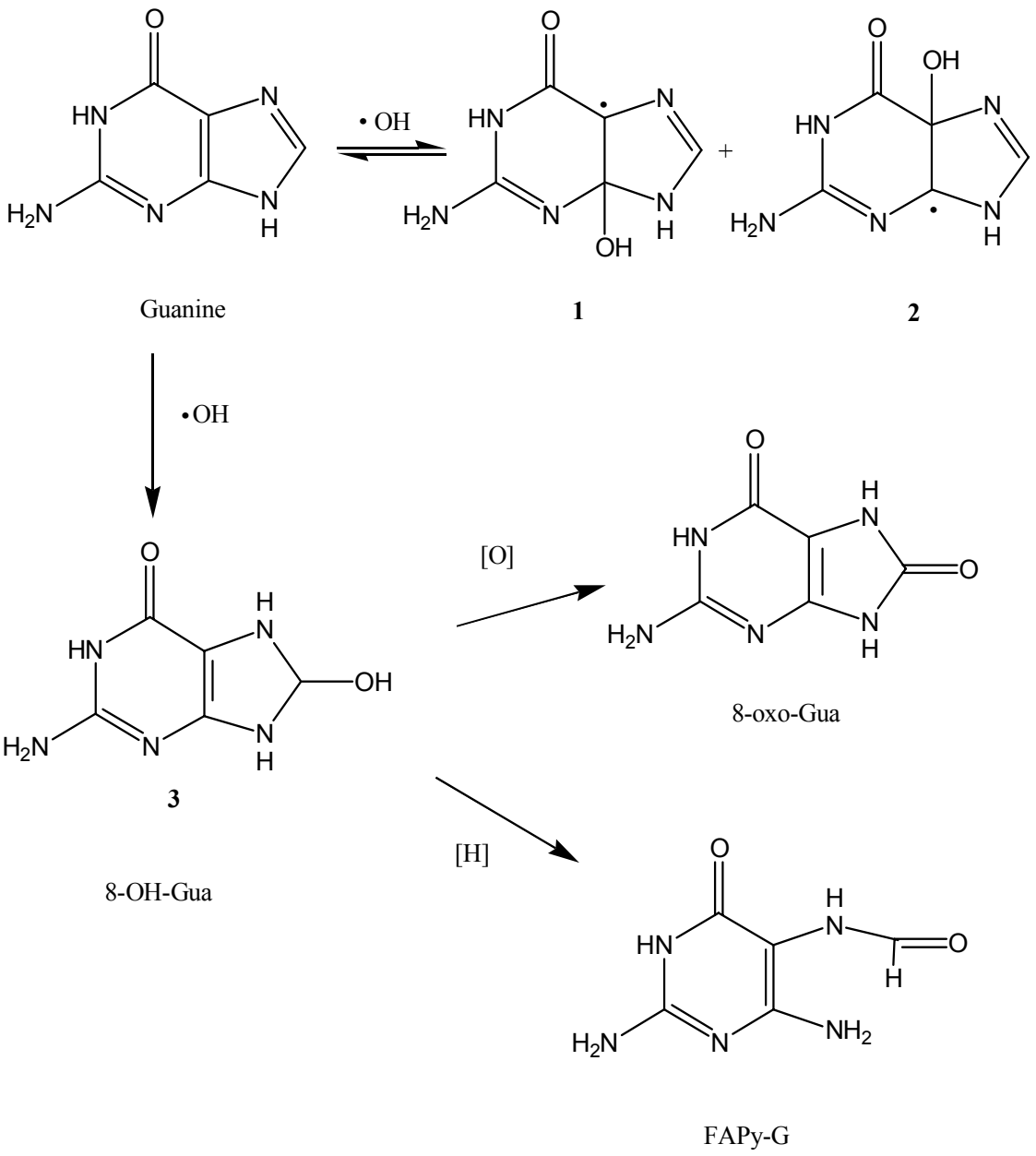

Figure 1.5 Schematic representation for the reaction of guanine with hydroxyl radicals.

1.4.2 Carbon centered radicals

The study of DNA damage by carbon-centered radicals began with the discovery of enediyne antibiotics. Since then, several works have been published on this subject. A good example is works by Kashinge and co-workers that showed through EPR studies that carbon radicals generated from dihydropyrazines are effective in causing DNA cleavage.[32]

There are two ways carbon centered radicals can be formed *in vivo*. One is under conditions of high oxidative stress and the other is by abnormal metabolism of carbohydrates and amino acids brought about by genetic disorders.

It is thought that alkyl radicals are able to abstract hydrogen atoms from the sugar moiety in nucleotides leading to alkylation and consequently DNA damage. Maeda and coworkers demonstrated that carbon radicals induced DNA damage by attacking guanine and adenine bases of DNA forming 8-alkylpurines which can ultimately lead to DNA damage (Figure 1.6).[33]

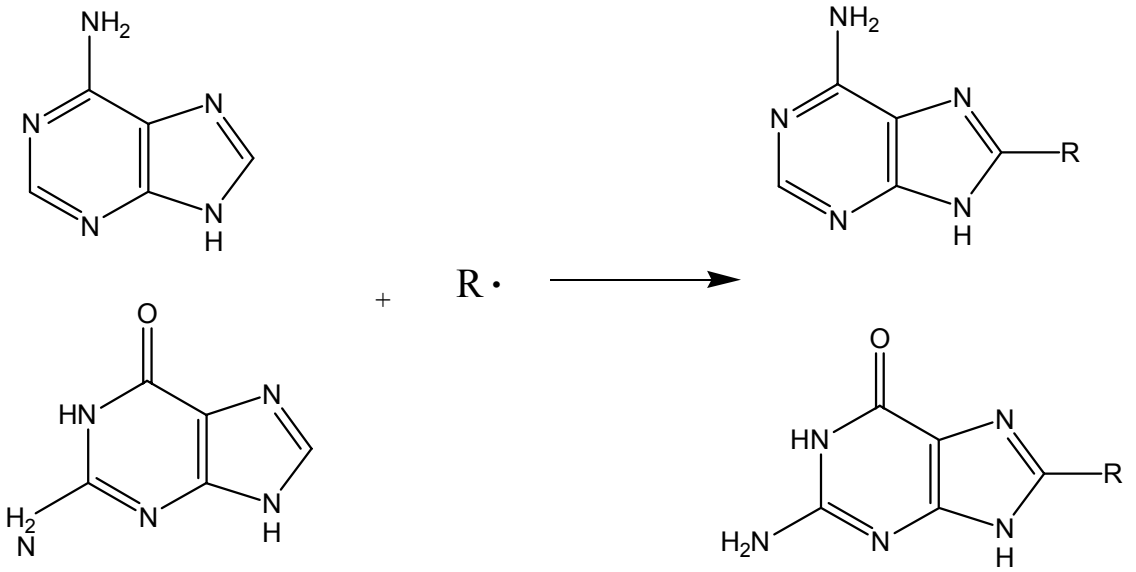

8-alkylated purines

Figure 1.6 Schematic representation of carbon centered metabolites where **R** represents a carbon radical.

1.5 Scope of the thesis

Previously, our laboratory has shown that $[(phen)_2Ru(tatpp)Ru(phen)_2]^{+4}$ ($\mathbf{P^{4+}}$) can damage DNA under both aerobic an anaerobic conditions. What makes $\mathbf{P^{4+}}$ unique is the fact that we see enhanced cleavage under anaerobic conditions compared to that of aerobic conditions.

Chapter 2 examines the photochemistry of $\mathbf{P^{4+}}$ in the presence and absence of DNA at different pH ranging from pH 6.0 – 11.0, and also examines the effect of DNA binding to the length of the excited state, **P***. In the second half of Chapter 2, we examine the effect of photo irradiating $\mathbf{P^{4+}}$ in the presence of DNA and observing any change in the DNA cleavage.

Chapter 3 discusses the effect of both oxygen and carbon radicals on our system. In the presence of oxygen, we observe that ROS do not play a role in the DNA cleavage mechanism. Under hypoxic conditions, complete quenching of our system in the presence of a carbon radical quencher was observed. We postulate that a carbon based radical species of $\mathbf{P}^{4+}$ may be responsible for the enhanced cleavage seen under anaerobic conditions.

CHAPTER 2

PHOTOCHEMISTRY OF $[Ru_2(phen)_4(tatpp)]Cl_4(P^{4+})$ IN PRESENCE AND ABSENCE OF DNA

2.1 Introduction

Over the past several years, studies on the interaction of polypyridyl Ru (II) complexes with DNA have been the focus of several research works. Ru (II) polypyridyl complexes are of particular interest due to a combination of stability, ease of construction, chirality and electronic properties.[10,34,35]

The dinuclear ruthenium complex, $[(phen)_2Ru(tatpp)Ru(phen)_2]^{+4}$ ($\mathbf{P^{4+}}$), where phen is 1,10 phenathroline and tatpp is 9,11,20,22-tetraaza,tetrapyrido[3,2,-*a*:2'3-*c*:3",2"-*l*:2"'3"'-*n*]-pentacene, has been synthesized in our laboratory. A ladder scheme has been constructed with the redox and protonation states of the tatpp bridging ligand in complex $\mathbf{P^{4+}}$ (scheme 1) with a corresponding shorthanded notation ($\mathbf{P^{4+}}$, $\mathbf{P^{3+}}$, $\mathbf{H_2P^{4+}}$ etc). The electron–transfer processes are presented vertically while protonation/ deprotonation processes are presented horizontally. [36]

The seven distinct species in this ladder scheme have been generated chemically or electrochemically and have been characterized by UV-Vis spectroscopy (Figure 2.1).[37]

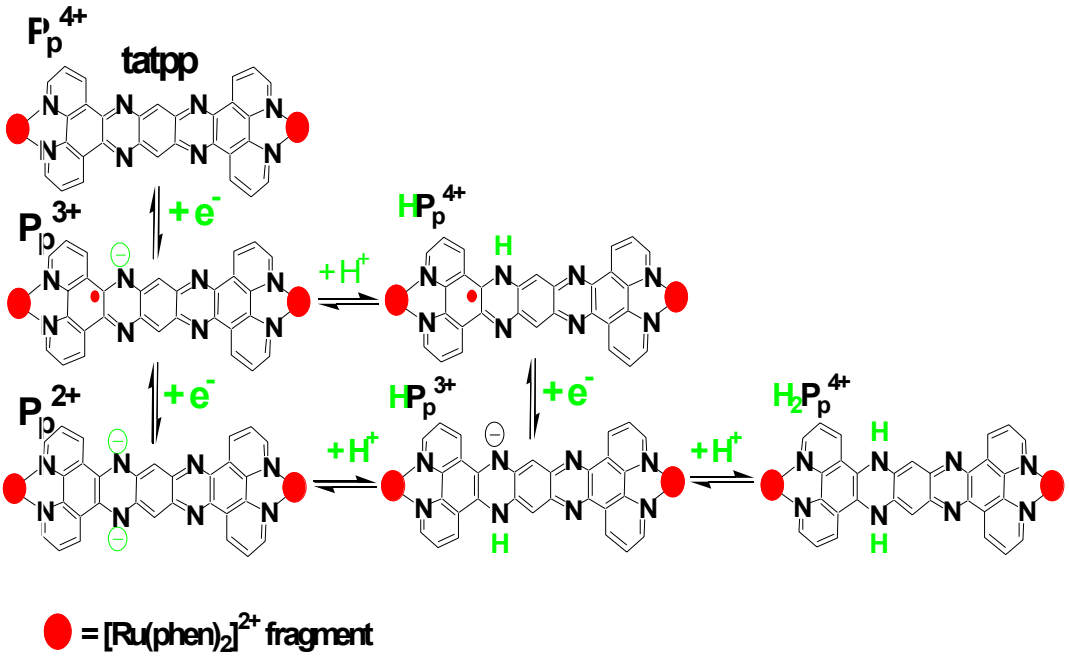

Scheme 1: Schematic diagram showing different redox and protonation steps of $\mathbf{P^{4+}}$.

The species show characteristic Ru-phen (dπ-π*) MLCT transitions at ~440 nm and unique LC transitions at longer wavelengths. The absorption spectra for the singly and doubly reduced species, $\mathbf{P^{3+}}$ and $\mathbf{P^{2+}}$ are shown in Figure 2.1a and are characterized by LC transitions that occur at long wavelengths (855 and 970 nm for $\mathbf{P^{3+}}$ and 635 and 685 nm for $\mathbf{P^{2+}}$). The absorption spectra for the protonated products are shown in Figure 2.1 b. Protonation of $\mathbf{P^{3+}}$ gives $\mathbf{HP^{3+}}$ and is characterized by a new peak at 715 nm in the spectrum of $\mathbf{P^{3+}}$ with a blue shift of the other LC bands to 655 nm and 608 nm. Addition of another proton yields $\mathbf{H_2P^{4+}}$ in which the LC transition appears as a new peak at 580 nm. $\mathbf{H_2P^{4+}}$ can be further reduced to $\mathbf{H_2P^{2+}}$.

.

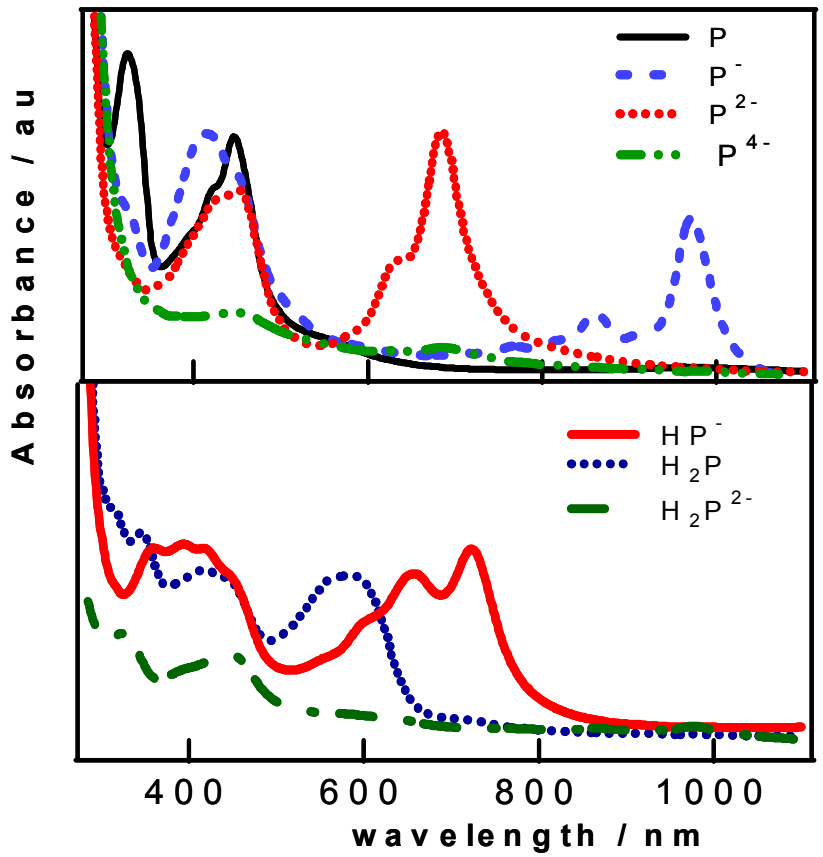

Figure 2.1: Top half: Absorption spectra of $\mathbf{P^{4+}}$after addition of 1.0 molar equiv of cobaltocene (dashed line, $\mathbf{P^{3+}}$) and 2.0 molar equiv of cobaltocene (dotted line, $\mathbf{P^{3+}}$) in degassed acetonitrile. Bottom half: Absorption spectra of $\mathbf{P^{3+}}$ after addition of 1.0 equiv of TFA (solid line, $\mathbf{HP^{4+}}$) degassed acetonitrile.

The photochemistry of $\mathbf{P^{4+}}$ at different pH's has been studied in water (Figure 2.2).[38] At pH 11.0, visible irradiation of $\mathbf{P^{4+}}$ results in the appearance of two absorption peaks at 970 and 860 nm which correspond to the formation of $\mathbf{P^{3+}}$ (Figure 2.2a_1). As these absorption bands begin to decrease in intensity, we see the formation of two new peaks at 635 and 725 nm which correspond to the formation of $\mathbf{HP^{3+}}$and $\mathbf{P^{2+}}$ respectively (Figure 2.2a_2). When decreasing the pH to 8.5, the formation of non-protonated $\mathbf{P^{3+}}$ is observed as the first photoreduced product and $\mathbf{HP^{3+}}$ is the dominant

protonated species with some residual amount of $\mathbf{P}^{2+}$still being formed but not the extent as that observed in pH 11.0 (Figure 2.2 b_1 and b_2).

At pH ~7.0, minor amounts of $\mathbf{P}^{3+}$ is initially formed as observed by its characteristic band at 970 nm. As the band at 970 nm continues to increase in intensity, the formation of a new peak at 580 nm is observed, which is consistent with the formation of $\mathbf{H_2P}^{4+}$ (Figure 2.2c).

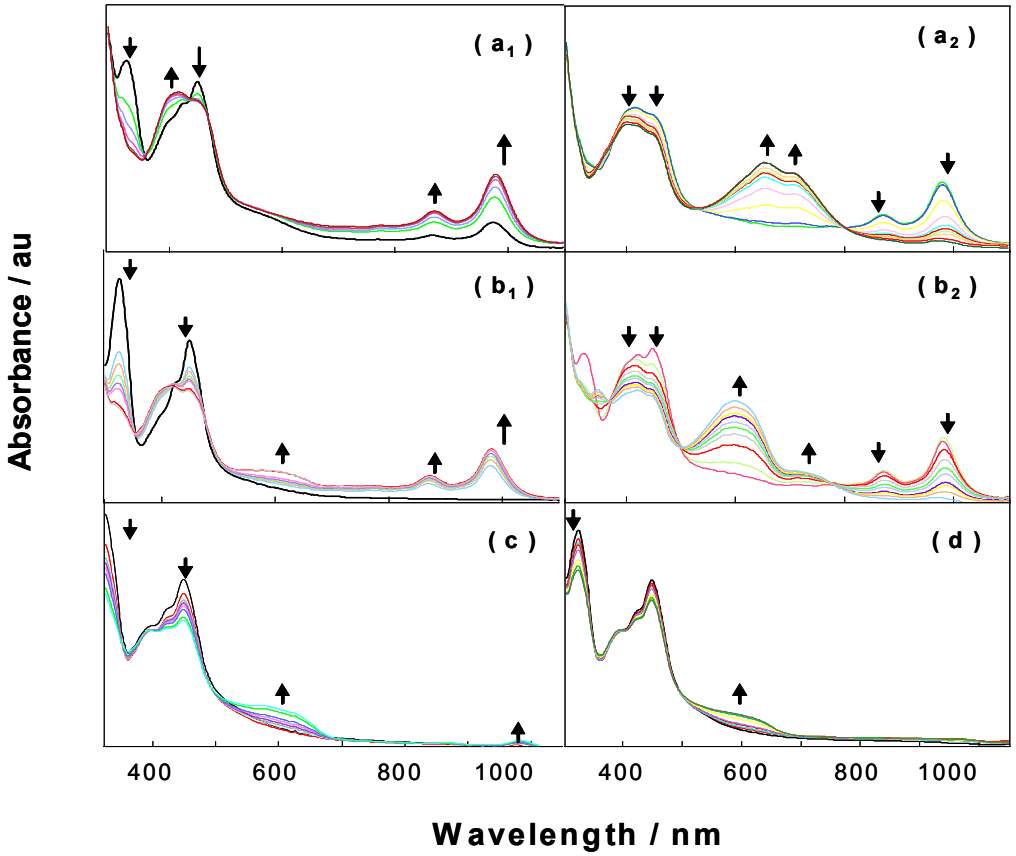

Figure 2.2: Evolution of the visible spectrum of 16 µM of $\mathbf{P}^{4+}$ in water with 0.25 M of TEOA during photolysis at four different pH values: pH 11 (a1 and a2), pH 8.5 (b_1 and b_2), and pH 7.0 (c) and pH 6.0 (d).

The multi-electron reduction under photochemical conditions of complex $\mathbf{P}^{4+}$ at pH $\geq$ 6.0 occurs according to equations (1) and (2) with the rate being expressed by equation (3)

$$\mathbf{P}^{4+} + h\nu \rightarrow \mathbf{P}^{*} \qquad (1)$$

$$\mathbf{P}^{*} + TEOA \rightarrow \mathbf{P}^{3+} + TEOA^{+} \qquad (2)$$

$$Rate_{2} = k\,[\mathbf{P}^{*}]\,[TEOA] \qquad (3)$$

As the lifetime ($t_{1/2}$) of **P*** increases, its probability of reacting with TEOA increases and therefore the reaction rate increases as would be expected by the rate law (rxn. 3). It was found that the $t_{1/2}$ of $\mathbf{P}^{*}$ is approximately 1.3 μs in dichloromethane, 4.5 ns in acetonitrile and less than 1 ns in water.[39] It will be worthy to compare the photochemistry of $\mathbf{P}^{4+}$ free vs. $\mathbf{P}^{4+}$ intercalated into DNA. Would the $t_{1/2}$ of **P*** be longer when it is intercalated into DNA? Would the bound form of $\mathbf{P}^{4+}$ be protected from the solvent and experience a more hydrophobic environment that induces a longer $t_{1/2}$ of its excited state? We hypothesize that the $t_{1/2}$ will be longer for the complex intercalated into DNA. This is because the bound form of $\mathbf{P}^{4+}$ will be protected from the solvent and experience a more hydrophobic environment like that experienced in dichloromethane. We hypothesize that $\mathbf{P}^{*}$ will be stabilized in a more hydrophobic environment and will therefore exhibit a longer $t_{1/2}$. We thus expect to see a faster photochemically reduction of $\mathbf{P}^{4+}$ to $\mathbf{P}^{3+}$ in the presence of DNA than for $\mathbf{P}^{4+}$ alone in solution.

2.1.1 Photocleavage of nucleic acids

Interactions of ruthenium polypyridyl complexes with DNA have been extensively studied over the past few years. Their unique binding properties as well as their photoactivity make them suitable candidates as DNA site-specific photocleavers.[40] Works by Barton et al. and Kelly et. al. have shown that simple ruthenium based compounds such as $[Ru(bpy)_3]^{2+}$ and $[Ru(phen)_3]^{2+}$ (Figure 2.3) are effective in bringing about significant damage to calf thymus DNA in as little 15 seconds.[40,41] These compounds are thought to initiate DNA cleavage *via* singlet oxygen species generated from the photoirradiation of the complexes. Interestingly, works carried out by Kelly et al. show that $[Ru(terpy)_2]^{2+}$ (Figure 2.3) is incapable of bringing about damage to calf thymus DNA.[40] O'Reilly, Kelly and Kirsch-De Mesmaeker linked two ruthenium monomers and found that these complexes exhibited ~100 fold enhancement in photonicking of supercoiled DNA (Figure 2.3).[42] This suggests that ligands do play a significant role when it comes to DNA photocleavers.

Most works on ruthenium complexes, such as those carried out by Barton on co-workers on ruthenium based complexes show that oxygen and light irradiation is essential for appreciable DNA cleavage. [43]

In the first half of chapter, we will investigate the rate of the photochemical reduction of $\mathbf{P^{4+}}$ in the presence and absence of DNA as a function of pH. We will examine the $t_{1/2}$ of **P*** by measuring the time it takes for the peaks associated with $\mathbf{P^{3+}}$ to increase in intensity the presence and absence of DNA and try to observe and if this $t_{1/2}$

is extended in this protected environment. In the second half of the chapter, we will examine the effect of white light on DNA damage.

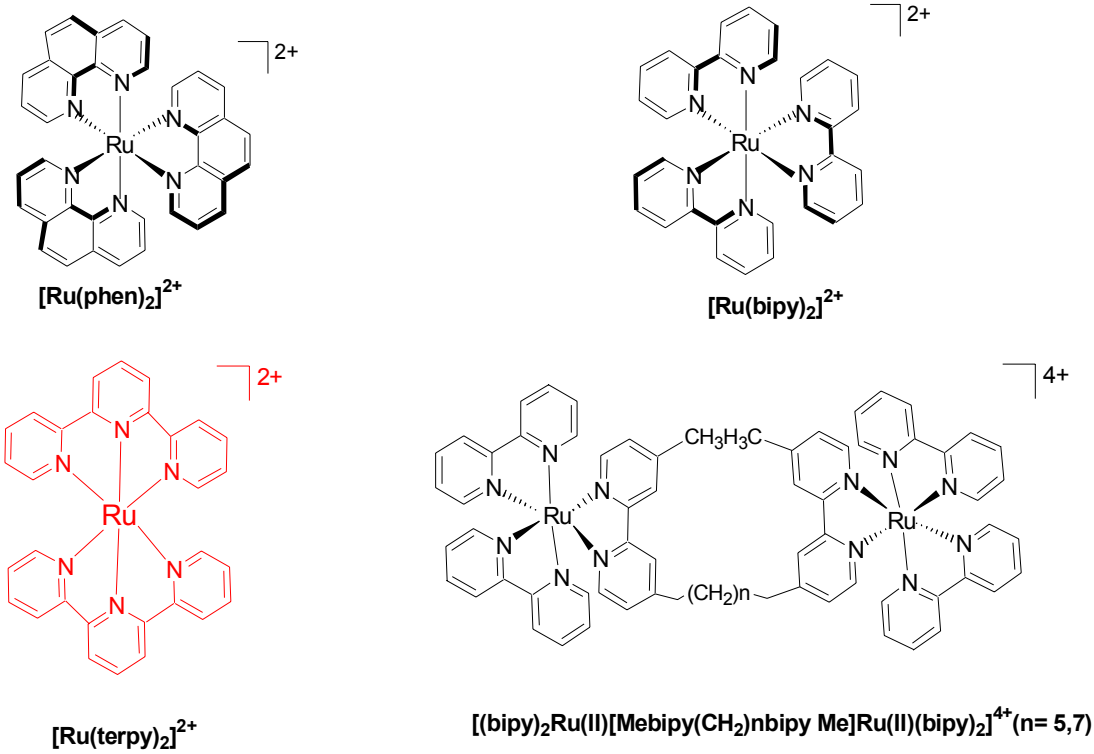

Figure 2.3 Some common Ru (II) photocleaving agents.

2.2 Results and discussion

2.2.1 Photoreduction of P^{4+} in the presence and absence of DNA at different pH

As shown in Figure 2.4a, the absorption spectrum of $\mathbf{P}^{4+}$ (16 μM) in aqueous buffered solution containing TEOA (0.10 M) as it is irradiated with visible light (λ > 330 nm) at pH 11.0. At pH 11.0, in the absence of DNA, we observe a small amount of $\mathbf{P}^{3+}$ is formed prior to irradiation which is denoted by the black line. We associate

this to the thermal formation of $\mathbf{P^{3+}}$. Upon further irradiation, (Figure 2.4b) longer wavelength peaks at 855 and 965 nm begin to decrease in intensity as peaks at 715 nm and 655 nm with a shoulder at 608 nm begin to increase in intensity. The second photoproduct can be assigned as a mixture of singly protonated, singly reduced $\mathbf{HP^{3+}}$ and the non-protonated $\mathbf{P^{2+}}$.

When the same experiment was performed in the presence of DNA ($\mathbf{P^{4+}}$:DNA ratio is 1:12), similar changes are observed although the process was slower overall. Upon irradiation, the two long wavelength peaks (855 and 965 nm) associated with $\mathbf{P^{3+}}$ increase in intensity (Figure 2.4c). Interestingly, these peaks do not increase in intensity to the same extent as observed in the absence of DNA. As the long wavelength peaks associated with $\mathbf{P^{3+}}$ began to decrease in intensity, we see the formation of new peaks at approximately at 655 and 715 nm and a shoulder at 608 nm. Due to the similarity of the spectrum of $\mathbf{P^{4+}}$ in the absence of DNA, these peaks are assigned to $\mathbf{HP^{3+}}$ and non protonated $\mathbf{P^{2+}}$. Their intensity is ca. 35-40% of that without DNA. Importantly, the time required for the full formation of $\mathbf{P^{3+}}$ was only 30 sec in buffered solution as compared to solutions containing excess DNA (DNA bp/$\mathbf{P^{4+}}$ ratio, 12:1) that took 120 sec.

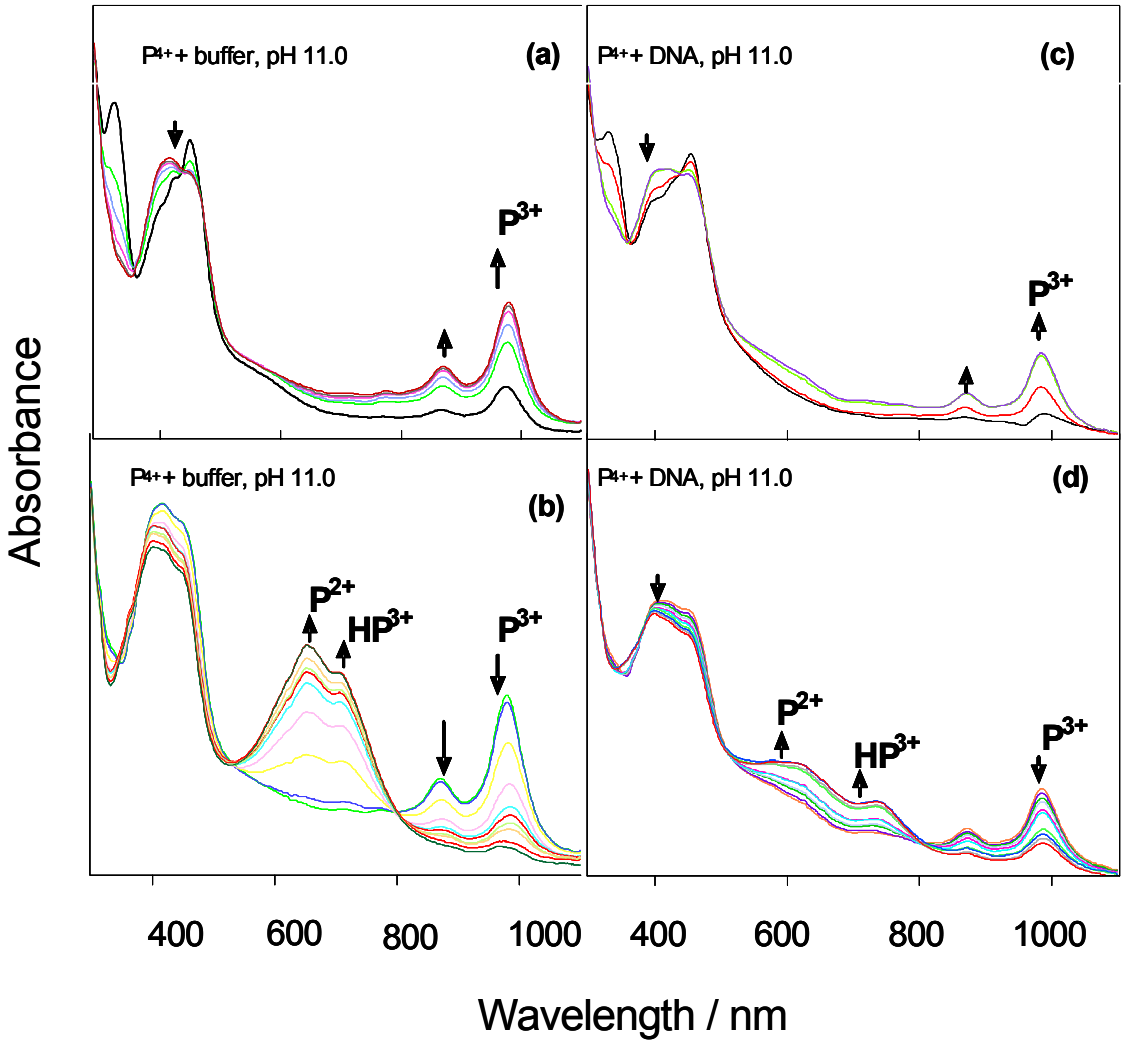

Figure 2.4: Absorption spectra of $\mathbf{P}^{4+}$ (16 μM) and TEOA (0.1 M) in the presence and absence of DNA (0.54 mM) at pH 11.0 (a) growth of $\mathbf{P}^{3+}$ in water, (b) growth of $\mathbf{HP}^{3+}$ and $\mathbf{P}^{2+}$ in water, (c) growth of $\mathbf{P}^{3+}$ with DNA, (d) growth of $\mathbf{P}^{3+}$ and $\mathbf{P}^{2+}$ with DNA. UV cutoff filter (< 360 nm), distance between light source and sample = 3 cm, at 18 ^{o}C.

Figure 2.5 shows the time plots for the different rates of formation of $\mathbf{P}^{3+}$ in the presence and absence of DNA. As shown in Figure 2.5, the time taken for the formation of $\mathbf{P}^{3+}$ is significantly slower in the presence of DNA as compared to that in the absence of DNA.

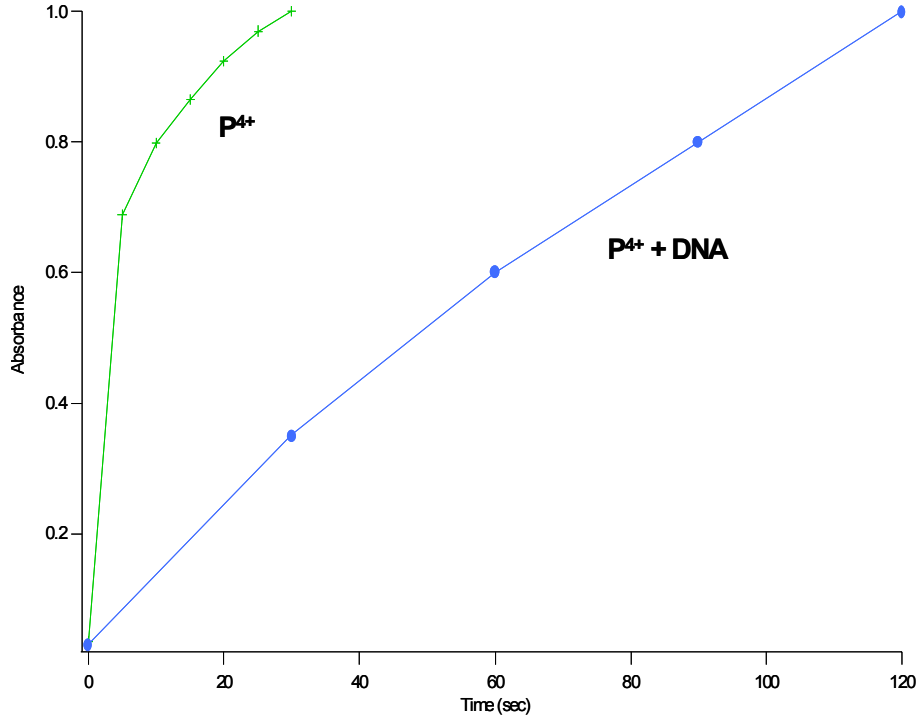

Figure 2.5: Rate of formation of $\mathbf{P}^{3+}$ in the presence and absence of DNA at pH 11.0.

At pH 8.5, in the absence of DNA, no thermal reaction with TEOA is observed. Upon irradiation, the two long wavelength peaks (855 and 965 nm) associated with $\mathbf{P}^{3+}$ (Figure 2.6a) increase in intensity with an additional peak appearing simultaneously at

580 nm. As the long wavelength peaks associated with $\mathbf{P^{3+}}$ reach a maximum and begin to decrease in intensity, the additional peak at 580 nm increases in the peak intensity indicating conversion to $\mathbf{H_2P^{4+}}$ (Figure 2.6b). The formation of a shoulder at 715 nm indicates that a small portion of $\mathbf{HP^{3+}}$ is also formed in this photoreaction.

In the presence of DNA, at pH 8.5, upon irradiation, we once again see the formation of the peaks associated with $\mathbf{P^{3+}}$ (Figure 2.6a). Interestingly, the peak associated with $\mathbf{P^{3+}}$ never increases in intensity to the full extent as in pH 11.0 and continues to grow throughout the experiment. This could be attributed to the fact that $\mathbf{P^{3+}}$ may somehow be reacting with the DNA through a process that is not well understood at this time. The appearance of a new peak at approximately 655 nm is also observed which remains to be investigated (Figure 2.6d). The time taken for the formation of $\mathbf{P^{3+}}$ was considerably longer in the presence of DNA (~17 min) compared to that in just solution (~30 sec). The fact that we see a much longer time for the formation of $\mathbf{P^{3+}}$ in the presence of DNA could be attributed to the formation of dimmers of $\mathbf{P^{3+}}$ (scheme 2). These dimmers can aggregate and further protect **P***, hence we see a longer $t_{1/2}$ as compared to pH 11.0. These dimmers may then undergo multiple reduction and protonaion states to form $\mathbf{H_2P^{4+}}$.

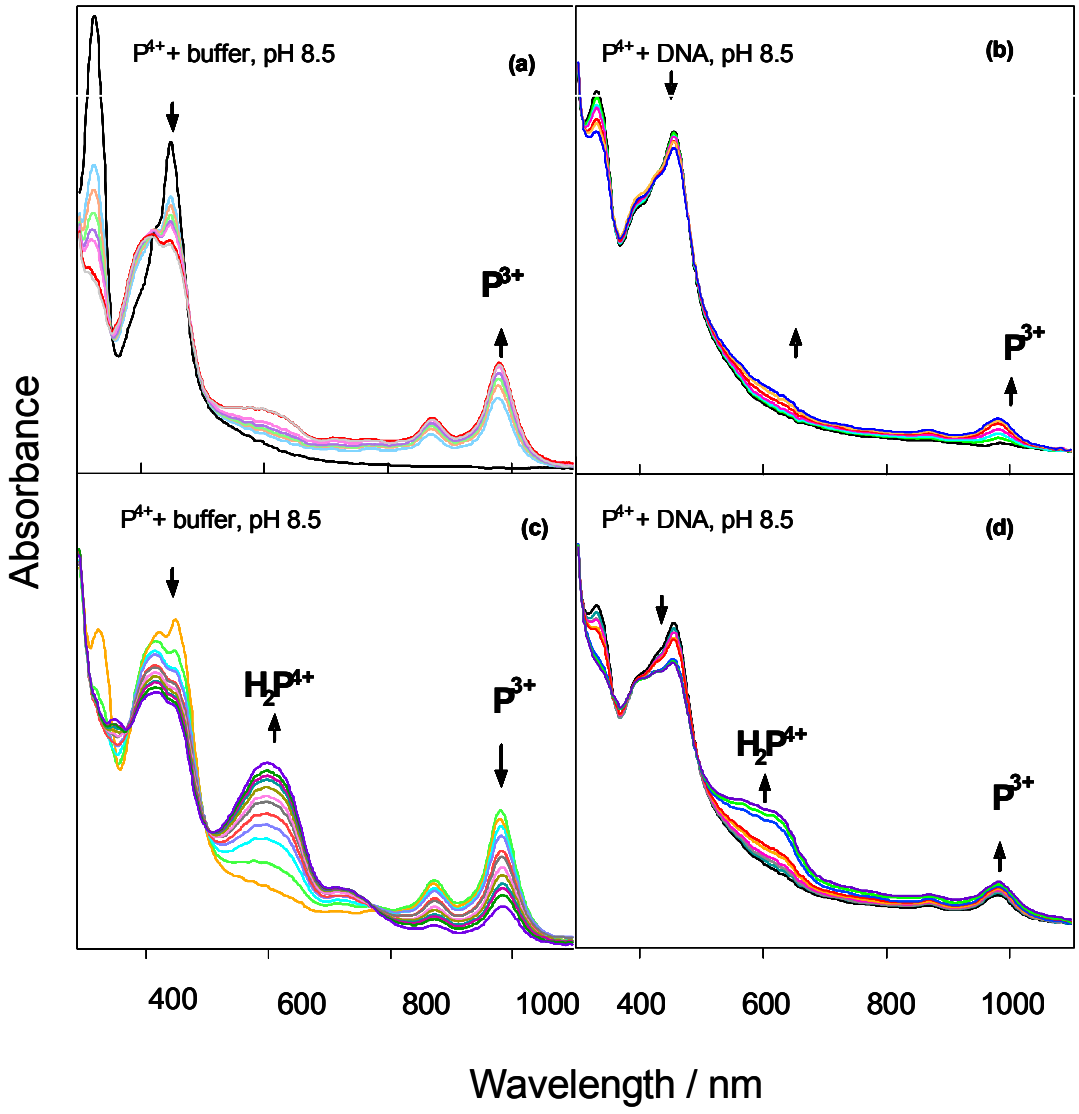

Figure 2.6: Absorption spectra of $\mathbf{P}^{4+}$ (16 μM) and TEOA (0.1 M) in the presence and absence of DNA (0.54 mM) at pH 8.5. (a) growth of $\mathbf{P}^{3+}$ in water, (b) growth of $\mathbf{H_2P}^{4+}$ in water, (c) growth of $\mathbf{P}^{3+}$ with DNA, (d) growth of unidentified species with DNA. UV cutoff filter (< 360 nm), distance between light source and sample = 3 cm, at 18 ^{o}C.

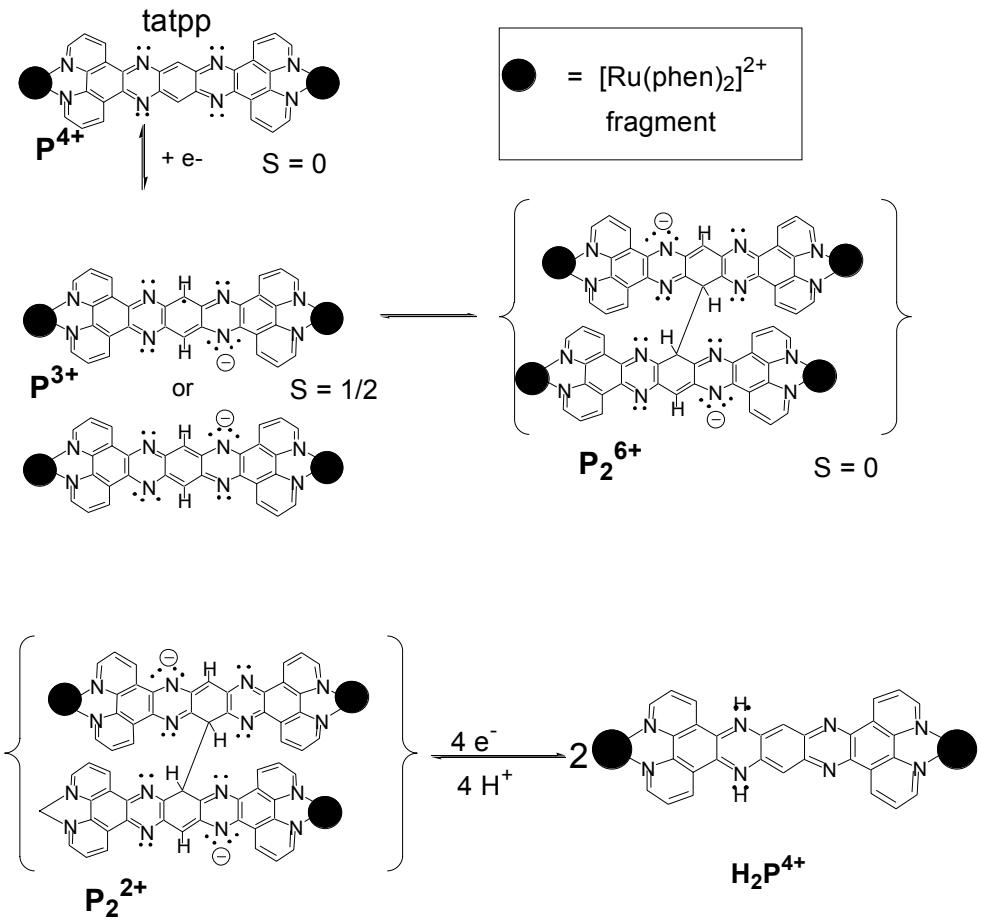

Scheme 2: Proposed model for the formation of $\mathbf{P^{3+}}$ dimmers and their conversion to $\mathbf{H_2P^{4+}}$.

At pH 7.0, in the absence of DNA (Figure 2.7a), only a small amount of $\mathbf{P^{3+}}$ is formed and the broad absorption at 580 nm begins to appear immediately, which is indicative of the formation of $\mathbf{H_2P^{4+}}$. Interestingly, this peak never increases in intensity to the same extent as that seen at pH 8.5, suggesting that there is direct photoreduction of $\mathbf{P^{4+}}$ (eq. 4) hence that is why we see the formation of $\mathbf{P^{4+}}$ and $\mathbf{H_2P^{4+}}$ only.

$$P^{4+} + 2e^- + 2H^+ \rightarrow H_2P^{4+} \qquad (4)$$

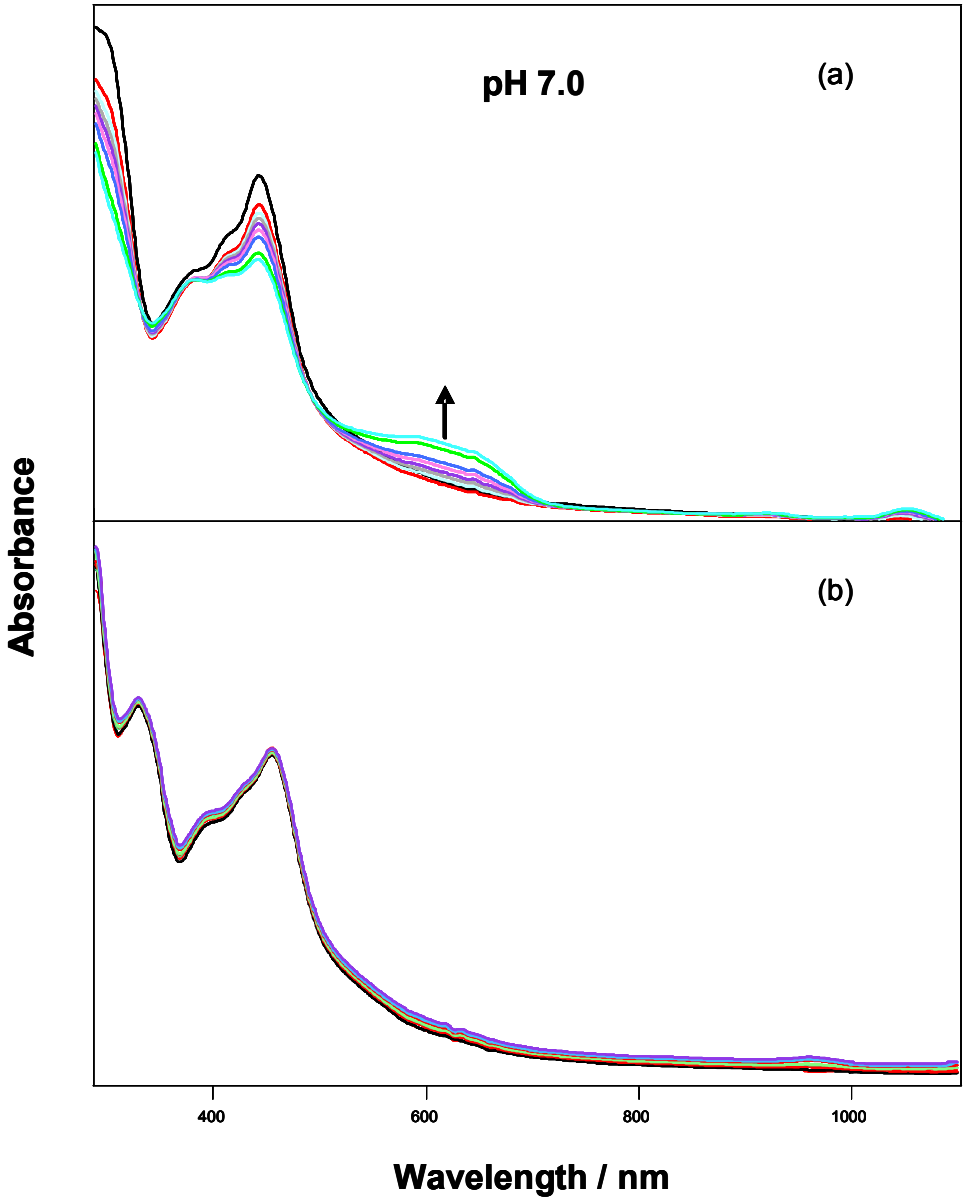

Figure 2.7: Absorption spectra of $\mathbf{P}^{4+}$ (16 μM) and TEOA (0.1 M) at pH 7.0. (a) in buffer (b) in the presence of DNA ($\mathbf{P}^{4+}$: DNA ratio is 1:12). UV cutoff filter (< 360 nm), distance between light source and sample = 3 cm, at 18 ^{o}C.

Notably, at pH 7.0 in the presence of DNA, none of the photoproducts are observed suggesting that complex $\mathbf{P^{4+}}$ intercalated into DNA is photochemically inactive at this pH.

At pH 6.0, in the absence of DNA, there is no trace of $\mathbf{P^{3+}}$ being formed. At shorter wavelengths, we do observe the growth of a broad peak that appears at 580 nm which is associated with $\mathbf{H_2P^{4+}}$. However, this peak never increases in intensity to the same extent as that observed at the higher pHs.

In the presence of DNA at pH 6.0, no photoproducts are observed. There are several possibilities as to why $\mathbf{H_2P^{4+}}$does not fully form at lower pH. One possibility is pH induced aggregation which can alter the photophysical behavior. Another possibility is the TEOA reducing agent is unable to deliver two electrons simultaneously to support reaction (4).

Contrary to our initial hypothesis, complex $\mathbf{P^{4+}}$ bound to DNA takes a longer time to photochemically reduce to $\mathbf{P^{3+}}$. In order to explain the results, we have considered the possibility that perhaps [**P***] is not really decreased upon binding to DNA but that the number of interactions between **P*-DNA** (intercalated into DNA) and TEOA is much lower than in the case that *free* **P***. When **P*** is intercalated into a big molecule such as DNA, forming **P*-DNA,** the probability of successful interactions between **P*-DNA** and TEOA is expected to be much lower than in the absence of DNA where the *free* **P*** can easily interactions with TEOA, and hence the photochemistry behaves as if **P*-DNA** would have a shorter $t_{1/2}$ than *free* **P***. This is because the second order rate constant (eq. 3) is proportional to the sum of the diffusion coefficients

of the two species intervening in the reaction (TEOA and **P*-DNA** or TEOA and free **P*)**. The diffusion coefficient of **P*-DNA** (taken as that of DNA alone) is at least two order of magnitude smaller than that of free **P***; and hence the reaction rate is smaller for **P*-DNA** than for *free* **P***.

2.2.2 The effect of photoirradiation of P^{4+} on DNA damage

As has been demonstrated in literature, most ruthenium polypyridyl complexes show enhanced DNA damage in the presence of light. In the second half of this chapter, we wish to investigate the effect of white light on the cleavage abilities of our complex $\mathbf{P^{4+}}$.

There are three main topological forms that plasmid DNA can exist as the supercoiled form (Form I), the circular form (Form II) and the linear form, (From III). Single strand (ss) cleavage also know as nicking coverts supercoiled (form I) to circular DNA (Form II). Double-strand (ds) cleavage converts supercoiled DNA to linear DNA (Form III). The employed method used to detect the three forms of DNA fragments is agarose gel electophoresis. The gels are stained with ethidum bromide and visualized under UV light (Figure 2.8).

The cleavage ability of our complex $\mathbf{P^{4+}}$ under normal room light irradiation has been extensively studied both under aerobic and anaerobic conditions. It has been found that $\mathbf{P^{4+}}$ in the presence of a reducing agent such as glutathione (GSH) can induce ss breaks thereby converting supercoiled DNA into circular DNA under aerobic conditions. Interestingly enough, under anaerobic conditions, we observe the complete

conversion of supercoiled DNA into circular DNA showing that DNA cleavage of $\mathbf{P^{4+}}$ is enhanced in the absence of oxygen.[44]

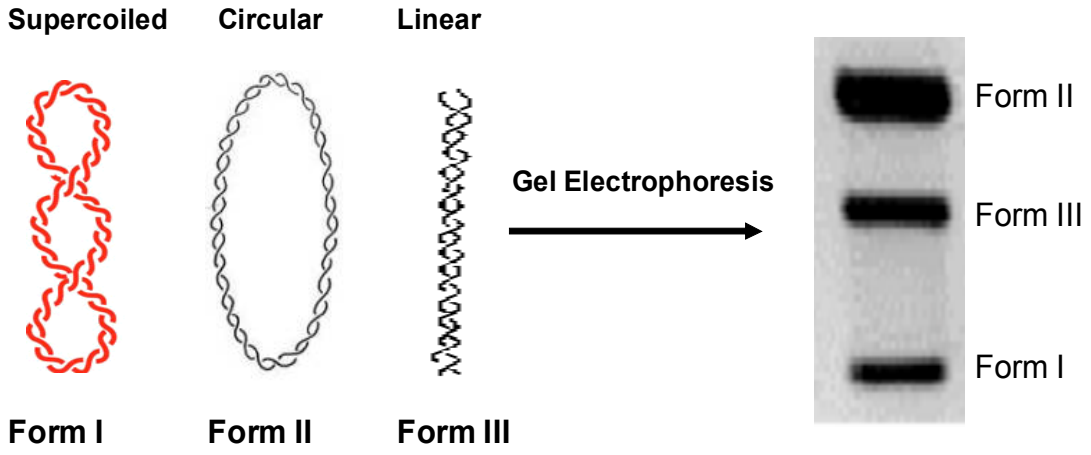

Figure 2.8: Topoisomers of plasmid DNA and how these three forms can be tracked using agarose gel electrophoresis.

2.2.3 Effect of white light on the DNA cleavage ability of P^{4+} in the presence of oxygen

The effect of photoirradiation of $\mathbf{P^{4+}}$ on DNA damage under aerobic conditions was examined. Two experiments were performed. The first experiment involved the incubation of $\mathbf{P^{4+}}$, GSH and pUC18 plasmid DNA at a ratio of 1:12 $\mathbf{P^{4+}}$ to DNA base pairs. Both sets of solutions were irradiated for 4 h with samples being taken after every hour. The second experiment involved identical solutions under identical experimental conditions as those in the first assay with the exception of the samples being incubated in a dark environment. After completion on the experiment, the

samples were quenched by the additions of ethanol and analyzed using gel electrophoresis.

The DNA cleaving activity of $\mathbf{P^{4+}}$ after irradiation with visible light ($\lambda_{irr} \geq 395$) was observed using gel electrophoresis (Figure 2.9). Control experiments (lanes 1 and 2) indicate that the effect of visible light does not induce any DNA damage. If we compare lanes 3-6 which are $\mathbf{P^{4+}}$ samples that have been irradiated for 1, 2, 3 and 4 h respectively, we observe no difference in $\mathbf{P^{4+}}$ induced DNA damage.

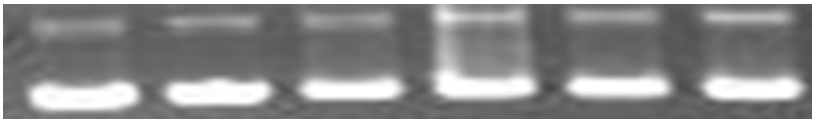

	1	2	3	4	5	6
$\mathbf{P^{4+}}$	+	+	+	+	+	+
hν	0	0	1 h	2 h	3 h	4 h

Figure 2.9: Agarose gel (1%) stained with ethidium bromide of supercoiled pUC18 DNA (0.154 mM) cleavage products after incubation at 25 ^{o}C for 4 h after irradiation with $\mathbf{P^{4+}}$ in 7 mM Na_3PO_4 buffer (pH 7.0). Lane 1: DNA control ; Lane 2: DNA plus $\mathbf{P^{4+}}$ (0.0128 mM); Lane 3: DNA plus $\mathbf{P^{4+}}$ (0.0128 mM) 1 h irradiation; Lane 4: DNA plus $\mathbf{P^{4+}}$(0.0256 mM) 2 h irradiation; Lane 5: DNA plus P^{4+}(0.0128 mM) 3 h irradiation; Lane 6: DNA plus $\mathbf{P^{4+}}$(0.0128 mM) 4 h irradiation.

The DNA cleaving ability of $\mathbf{P^{4+}}$ in the dark was also tested. As can be observed in Figure 2.10, lanes 3-6, there is no cleavage activity as compared to the control lanes 1 and 2.

The DNA cleavage activity of $\mathbf{P^{4+}}$, GSH and DNA in the presence and absence of visible light ($\lambda_{irr} \geq 395$) was also investigated (Figure 2.11). Studies of $\mathbf{P^{4+}}$ and GSH in the presence of DNA under anaerobic conditions have previously conducted in our

laboratory and have been found to yield ~48% of circular DNA. Lanes 4-6, represent $\mathbf{P^{4+}}$ and GSH in the presence of DNA after 1, 2 and 3 h of irradiation respectively.

	1	2	3	4	5	6
$\mathbf{P^{4+}}$	+	+	+	+	+	+

Figure 2.10: Agarose gel (1%) stained with ethidium bromide of supercoiled pUC18 DNA (0.154 mM) cleavage products after incubation at 25 ^{o}C for 4 h with $\mathbf{P^{4}}$ in 7 mM Na_3PO_4 buffer (pH 7.0), no irradiation. Lane 1: DNA control; Lane 2: DNA plus $\mathbf{P^{4+}}$ (0.0128 mM; Lane 3: DNA plus $\mathbf{P^{4+}}$ (0.0128 mM) 1 h, no irradiation; Lane 4: DNA plus $\mathbf{P^{4+}}$(0.0128 mM) 2 h, no irradiation; Lane 5: DNA plus $\mathbf{P^{4+}}$ (0.0256mM) 3 h, no irradiation; Lane 6: DNA plus $\mathbf{P^{4+}}$(0.0128 mM) 4 h, no irradiation.

As observed, the presence of white light has no significant effect on the cleavage activity yielding ~55% of circular DNA. Interestingly, after 4 h of irradiation (lane 7), we see that a mixture of $\mathbf{P^{4+}}$ and GSH yields ~80% of circular DNA.

	1	2	3	4	5	6	7
$\mathbf{P^{4+}}$	-	+	+	+	+	+	+
GSH	-	-	+	+	+	+	+
hν	-	-	-	1 h	2 h	3 h	4 h

Figure 2.11: Agarose gel (1%) stained with ethidium bromide of supercoiled pUC18 DNA (0.154 mM) cleavage products after incubation at 25 ^{o}C for 4 h after irradiation with $\mathbf{P^{4+}}$ and GSH in 7 mM Na_3PO_4 buffer (pH 7.0). Lane 1: DNA control; lane 2: DNA plus $\mathbf{P^{4+}}$ (0.0128 mM); lane 3: DNA plus GSH (2.01 mM); lane 4: DNA,GSH (2.01 mM) plus $\mathbf{P^{4+}}$ (0.0128 mM), 1 h irradiation; lane 5: DNA,GSH (2.01 mM) plus $\mathbf{P^{4+}}$ (0.0128 mM), 2 h irradiation; lane 6: DNA,GSH (2.01 mM) plus $\mathbf{P^{4+}}$ (0.0128 mM), 3 h irradiation; DNA,GSH (2.01 mM) plus $\mathbf{P^{4+}}$ (0.0128 mM), 4 h irradiation.

The cleavage activity of $\mathbf{P^{4+}}$, DNA and GSH was also observed in the dark (Figure 2.12). Lanes 1-3 serve as controls. Lanes 4-7, which represent those samples that were photoirradiated for 1, 2, 3 and 4 h respectively, show no change in cleavage activity. Comparison of lane 7 in Figure 2.11 to lane 7 in Figure 2.12 show a significant difference with most of the supercoiled DNA being converted to circular after photoirradiation for 4 h.

	1	2	3	4	5	6	7
$\mathbf{P^{4+}}$	-	+	+	+	+	+	+
GSH	-	-	+	+	+	+	+

Figure 2.12: Agarose gel (1%) stained with ethidium bromide of supercoiled pUC18 DNA (0.154 mM) cleavage products after incubation at 25 ^{o}C for 4 h with $\mathbf{P^{4+}}$ and GSH in 7 mM Na_3PO_4 buffer (pH 7.0), no irradiation. Lane 1:DNA control; lane 2: DNA plus $\mathbf{P^{4+}}$ (0.0128 mM); lane 3: DNA plus GSH (2.01 mM); lane 4: DNA, GSH (2.01 mM) plus $\mathbf{P^{4+}}$ (0.0128 mM),1 h, no irradiation; lane 6: DNA, GSH (2.01 mM) plus $\mathbf{P^{4+}}$ (0.0128 mM), 2 h, no irradiation; DNA, GSH (2.01 mM) plus $\mathbf{P^{4+}}$ (0.0128 mM), 3 h, no irradiation; DNA, GSH (2.01 mM) plus $\mathbf{P^{4+}}$(0.0128 mM), 4 h, no irradiation.

Kelly et.al.[45,46] has shown that certain ruthenium complexes react with DNA *via* electron transfer. He showed that these complexes can induce spontaneous nicks in supercoiled DNA and form photoadducts with guanine residues that are readily oxidized. The single strand nicking that is observed in lane 7 (Figure 2.11) may be attributed to an electron transfer that might be occurring between the metal centre and the guanine residues as shown in the equation below.

$$P^{*} + G \longrightarrow P^{\bullet -} + G^{\cdot +}$$

2.2.4 Effect of white light on the DNA cleavage ability of P^{4+} in the absence of oxygen

Since $\mathbf{P^{4+}}$ in the presence of GSH has been found to show enhanced cleavage activity under hypoxic conditions, we wanted to examine the effect of visible light on cleavage activity of $\mathbf{P^{4+}}$ under anaerobic conditions in the presence and absence of light and with GSH. For comparison, similar experiments were conducted as those performed in section 2.2.1, with the exception of an oxygen free environment.

Figure 2.13 shows the agarose gel of photoirradiated $\mathbf{P^{4+}}$. Lanes 1 and 2 serve as controls whilst lanes 3-5 represent samples that contained $\mathbf{P^{4+}}$ after 1, 2, 3 and 4 h of photoirradiation respectively. As can be seen, we observe no difference in $\mathbf{P^{4+}}$ induced DNA damage. Similar results were obtained for $\mathbf{P^{4+}}$ in the dark.

	1	2	3	4	5	6
$\mathbf{P^{4+}}$	-	-	+	+	+	+
hν	-	-	1 h	2 h	3 h	4 h

Figure 2.13: Agarose gel (1%) stained with ethidium of supercoiled pUC18 DNA (0.154 mM) cleavage products after incubation at 25 ^{o}C for 4 h of irradiation with $\mathbf{P^{4+}}$ in 7 mM Na_3PO_4 buffer (pH 7.0) under anaerobic conditions. Lane 1: DNA control; Lane 2: DNA plus $\mathbf{P^{4+}}$ (0.0128 mM); Lane 3: DNA plus $\mathbf{P^{4+}}$ (0.0128 mM) 1 h irradiation; Lane 4: DNA plus $\mathbf{P^{4+}}$ (0.0128 mM) 2 h irradiation; Lane 5: DNA plus $\mathbf{P^{4+}}$ (0.0128 mM) 3 h irradiation; Lane 6: DNA plus $\mathbf{P^{4+}}$(0.0128 mM) 4 h irradiation.

The effect of white light on cleavage activity of $\mathbf{P^{4+}}$ and GSH was observed (Figure 2.14). Previous studies carried out on $\mathbf{P^{4+}}$ in the presence of GSH under anaerobic conditions showed enhanced cleavage with the complete conversion of supercolied

DNA to circular DNA. Lanes 1-3 serve as control lanes. Lanes 5-8 represent the samples that were photoirradiated after 1 h, 2 h, 3 h and 4 h respectively. In lane 8, we see the small formation a linear DNA. Though we cannot totally rule out the possibility role of white light, it seems likely that the small amount of linear DNA we observe in lane 8 can be attributed to random ds nicks. The same experiment was conducted under low light conditions and similar results were observed.

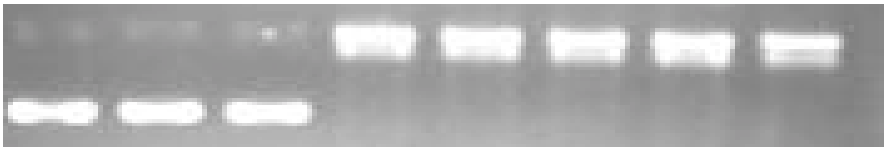

	1	2	3	4	5	6	7	8
$\mathbf{P^{4+}}$	-	-	+	+	+	+	+	+
GSH	-	+	+	+	+	+	+	+
hν	-	-	-	-	1 h	2 h	3 h	4 h

Figure 2.14: Agarose gel (1%) stained with ethidium bromide of supercoiled pUC18 DNA (0.154 mM) cleavage products after incubation at 25 ^{o}C for 4 h after irradiation with $\mathbf{P^{4+}}$ and GSH in 7 mM Na_3PO_4 buffer (pH 7.0) under anaerobic conditions. Lane 1:DNA control; lane 2: DNA plus $\mathbf{P^{4+}}$ (0.0128 mM); lane 3: DNA plus GSH (2.01 mM); lane 4: DNA, GSH (2.01 mM) plus $\mathbf{P^{4+}}$ (0.0128 mM); lane 5: DNA,GSH (2.01 mM) plus $\mathbf{P^{4+}}$ (0.0128 mM), 1 h irradiation; lane 6: DNA, GSH (2.01 mM) plus $\mathbf{P^{4+}}$ (0.0128 mM), 2 h irradiation; lane 7: DNA, GSH (2.01 mM) plus $\mathbf{P^{4+}}$ (0.0128 mM), 3 h irradiation; lane 8: DNA, GSH (2.01 mM) plus $\mathbf{P^{4+}}$ (0.0128 mM), 4 h irradiation.

2.3 Summary and conclusions

Our complex $\mathbf{P^{4+}}$ in the presence of a reducing agent such a TEOA was found to be photochemically active. At alkaline pH's, that is pH 11.0 and 8.5, we observed the formation of the photoproducts $\mathbf{P^{3+}}$, $\mathbf{H_2P^{4+}}$ in the absence of DNA. In the presence of DNA, at alkaline pH's, we observed the formation of $\mathbf{P^{3+}}$ and $\mathbf{HP^{3+}}$ and a new

species at 630 nm (pH 8.5) which we are yet to identify. At neutral pH, pH 7.0, we observed the small formation of $\mathbf{H_2P^{4+}}$ in the absence of DNA, and no photoproducts are observed in the presence of DNA.

In the absence of DNA in slightly acidic pH, only the slight formation of $\mathbf{H_2P^{4+}}$ is observed. No photoproducts are observed in the presence of DNA.

Interestingly, upon the examination of the $t_{1/2}$ **P***, we found that the $t_{1/2}$ of **P*** is not enhanced in the presence of DNA as we had expected. We attribute this to the decreased interactions of DNA bound $\mathbf{P^{4+}}$ with TEOA. In the absence of DNA, we found that the $t_{1/2}$ of **P*** is enhanced. We attributed this to the increased interactions of free $\mathbf{P^{4+}}$ with TEOA.

The effect of visible light on DNA damage was also examined. Through the various experiments conducted in the presence and absence of white light both under aerobic and anaerobic conditions; we have observed that visible light does not play a role in the DNA cleavage ability of $\mathbf{P^{4+}}$. We have shown that our system induces DNA damage through a light independent pathway.

2.4 Experimental

2.4.1 Chemicals

All reagents were purchased commercially and used without further purification unless noted. $[(phen)_2Ru(tatpp)Ru(phen)_2]Cl_4$ ($[\mathbf{P^{4+}}]Cl_4$) was synthesized according to literature methods. Millipore water was used to prepare all buffers. Supercoiled pUC18 DNA was purchased from Bayou Biolabs (New England). Agarose, ethidium bromide, glutathione (GSH), and Calf Thymus DNA were purchased from Sigma Aldrich. The DNA concentration was determined by absorption spectroscopy using the molar coefficient of (13,300 M^{-1} DNA-bp) at 260 nm.

2.4.2 Instrumentation

UV-visible spectra were obtained on a Hewlett-Packard HP8453A spectrophotometer and the light source used was a Stockel Yale Model 21AC fiber optic illuminator.

2.4.3 Photochemistry of P^{4+} *in water*

In a typical experiment, 665 μL of 16 μM $\mathbf{P^{4+}}$ and 114.6 μL of 0.1M of TEOA was transferred into a 3 mL glass cuvette and made to up 2.5 mL using 40 mM Tris buffer (pH 7.5). The solution was capped using a rubber septum and deoxygenated by bubbling with nitrogen for 10 min. The solution was then placed in a 25 ^oC water bath which was situated 3 cm way from the light source and was irradiated with white light. Measurements were taken after every 5 sec for the first minute and then 60 sec for the remaining time of the experiment.

In the DNA photochemistry experiment, a stock solution of calf thymus DNA was prepared by dissolving ~45 mg of Calf Thymus DNA in Buffer I (50 mM Tris, 100 mM NaCl, pH 7.5). The solution was centrifuged at 13,000 rpm for 10 min and resuspended in Buffer II (50 mM NaCl, 5 mM Tris, pH 7.5). An absorbance reading was taken at 260 nm and the DNA concentration was obtained using Beer's law.

In a typical experiment, 523 μL of 0.034 mM DNA , 665 μL of 0.016 mM $\mathbf{P^{4+}}$ and 114.6 μL of 0.1M of TEOA was transferred into a 3 mL glass cuvette and made to up 2.5 mL using 40 mM Tris buffer (pH 7.5). The solution was deagassed in the same way as described above and measurements were taken after every 5 sec for the first minute and then 60 sec for the rest of the experiment.

2.4.4 Photocleavage of pUC18 plasmid DNA

DNA photocleavage experiments where carried out in a total volume of 80 μL in 1 mL. Eppendorf tubes containing 20 μL of $\mathbf{P^{4+}}$ (0.0128 mM), 20 μL of GSH (1.02 mM) and 2 μL of pUC18 DNA (1 μg/1 μL), 0.154 mM DNA base pairs) in 7 mM Na_3PO_4 buffer medium (pH 7.0). Samples were irradiated using a 150W optical light source with a 360 nm UV filter. The distance between the sample Eppendorf and the light source was set at 3 cm. After every hour, 20 μL aliquots were taken and the DNA was then precipitated by adding 2 μL of 3 M sodium acetate (pH 5.2) and 80 μL of ethanol, followed by cooling at -20 ^{o}C overnight. The precipitated DNA was then centrifuged at 13,000 rpm (rounds per minute) for 30 min. The ethanol solution was decanted out of the Eppendorfs and dried under vacuum for 20 min. The samples were then resuspended in 30 μL storage buffer (40 mM Tris-Cl, 1 mM EDTA , pH 8.0) and

10 μL loading buffer (30% glycerol in millipore water with 0.1% w/v bromophenol blue). After that, 5 μL of each sample was loaded in a 1% agarose gel containing ethidium bromide (0.2 μL/1 mL) and then subjected to electrophoresis at 70 V for 2 h using TAE buffer (40 mM Tris-acetate, 1 mM EDTA, pH 8.0) as the running buffer. Bands were visualized by UV light and photographed with a UV illuminator.

2.4.5 Anaerobic reactions

Solutions of similar concentrations as those described in section 2.4.4 were degassed 4X using the freeze thaw method and then transferred into a nitrogen atmosphere glove box. Samples were irradiated with 150W optical light source with a 360 nm UV filter for 4 h with 20 μL aliquots taken after every hour. The distance between the sample Eppendorf and the light source was set at 3 cm. Samples were then precipitated anaerobically using 2 μL degassed 3 M sodium acetate (pH 5.2) and 80 μL degassed ethanol. The solutions were then subjected to subsequent precipitation and analysis steps similar to those in described 2.4.4.

CHAPTER 3

MECHANISM OF DNA CLEAVAGE WITH RUTHENIUM POLYPYRIDYL COMPLEXES

3.1 Introduction

Since the discovery of cisplatin as an effective chemotherapeutic agent, there has been intensive interest in the use of metal complexes as potential chemotherapeutic drugs. In particular, ruthenium complexes have been studied extensively as its chemical reactivity is quite similar, in many cases, to that of platinum complexes. In recent years, a few ruthenium complexes have demonstrated favorable anti-tumor properties whilst showing lower systemic toxicity than platinum (II) compounds. [18,19,47]

In addition, there are numerous reports on the binding and properties of cationic ruthenium polypyridyl complexes with DNA. Barton et. al. have shown that many such complexes, such as $[Ru(phen)_2dppz]^{2+}$,(Figure 3.1) bind DNA tightly via intercalation and fluoresce only when bound.[17] Lincoln and coworkers have shown that some dinuclear ruthenium complexes can bind DNA incredibly tightly, with binding constants on the order of 10^{11} M^{-1}, and that these complexes slowly thread their way through the DNA duplex.[48]

Despite these studies, cationic polypyridyl complexes have found little therapeutic applications, owing primarily to their toxicity at the organismal level. Dwyer showed that simple complexes such as $[Ru(phen)_3]^{2+}$ and $[Ru(bpy)_3]^{2+}$ are toxic to mice (via interperotoniel injection) at doses of 18.4 mg and 16 mg complex / kg

mouse body weight, respectively. He further showed that these complexes are potent inhibitors of acetylcholine esterase (AChE) which is their presumed biological target.[49]

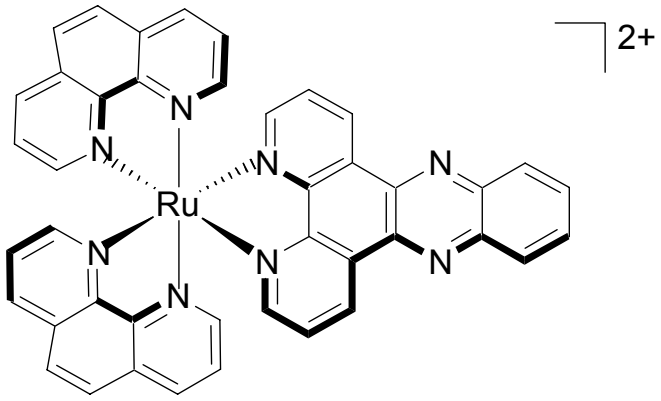

Figure 3.1: Structure of $[Ru(phen)_2dppz]^{2+}$ where phen is 1,10-phenathrolibne and dppz is dihydrophenazine

Recently, this lab showed that the dimeric ruthenium complex $\mathbf{P}^{4+}$ (Figure 3.2) has the ability to bind and cleave DNA and that this activity is potentiated under hypoxic (anaerobic) conditions.[50] Furthermore, this complex's toxicity towards mice (MTD ~67 mg/kg) was considerably less than that for $[Ru(phen)_3]^{2+}$ and $[Ru(bpy)_3]^{2+}$ suggesting these complexes may be useful therapeutically. It also seems likely that these complexes will be able to cross the cell membrane as just recently, Barton and co-workers showed that the cationic complex $[Ru(phen)_2dppz]^{2+}$ crosses the cell membrane.[51]

Of the few Ru (II) complexes found to damage DNA, all but $\mathbf{P}^{4+}$ require irradiation with visible light and these are postulated to function by oxidative quenching the ^{3}MLCT excited-state on the ruthenium complex by O_2 to form $O_2^{\bullet -}$ and other

reactive oxygen species (ROS).[52] These ROS are thought to abstract hydrogen from the sugar moiety found in nucleotides and thus bring about DNA damage.

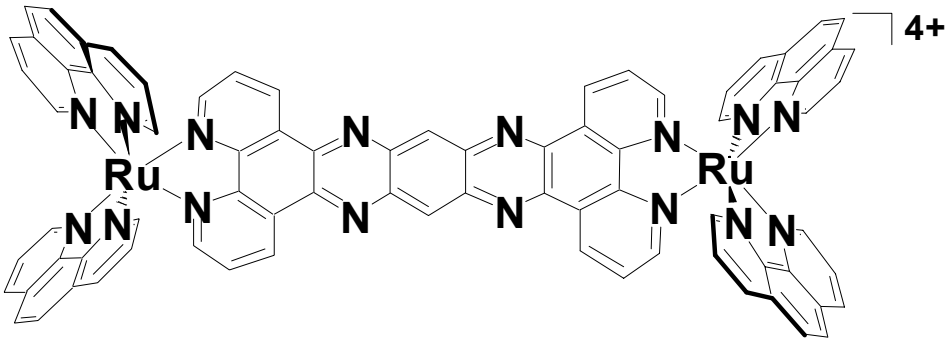

Figure 3.2: The dinuclear ruthenium complex, $[(phen)_2\ Ru\ (tatpp)Ru(phen)_2]^{+4}$ ($\mathbf{P^{4+}}$) where phen is 1,10 phenathroline and tatpp is 9,11,20,22-tetraaza, tetrapyrido [3,2,-a:2'3-(:3",2"-1:2"'3"') pentacene]

The cleavage activity of $\mathbf{P^{4+}}$, on the other hand, is attenuated under aerobic conditions suggesting a completely different mechanism for DNA damage. This enhanced activity under hypoxia could also prove useful therapeutically as hypoxic tumor cells are one of the most difficult subpopulations of cancer cells to effectively treat.

The ability of $\mathbf{P^{4+}}$ to cleave DNA was determined using a simple assay in which cleavage is followed by the conversion of supercoiled plasmid DNA (Form I) to circular DNA (Form II) upon single-strand (ss) cleavage or to linear DNA (Form III) upon double-strand (ds) cleavage. These three forms of DNA are separable by agarose gel electrophoresis and the results from such a study are shown in Figure 3.3.[50] As can be

seen, $\mathbf{P^{4+}}$ alone does not induce any significant DNA damage (lane 2). However, in the presence of GSH, $\mathbf{P^{4+}}$ does cause considerable nicking of the DNA (lane 4). Lane 5 shows the enhancement of this activity under anaerobic conditions.[50]

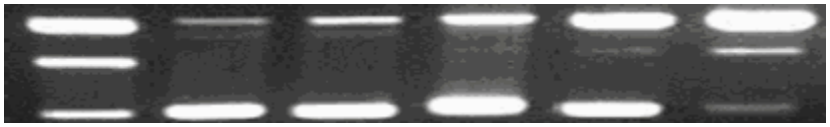

	M	1	2	3	4	5
$\mathbf{P^{4+}}$		-	+	-	+	+
GSH		-	-	+	+	+
$\mathbf{O_2}$		+	+	+	+	-

Figure 3.3: Agarose gel (1%) stained with ethidium bromide of supercoiled pUC18 DNA (0.154 mM) cleavage products after incubation at 25 ^{o}C for 2 h with $\mathbf{P^{4+}}$ and GSH in 7 mM Na_3PO_4 buffer (pH 7.0). Lane M, marker lane containing form I, II and III DNA. Lane 1: DNA control; Lane 2: DNA plus $\mathbf{P^{4+}}$ (0.0128 mM); Lane 3: DNA plus GSH (0.513 mM); Lane 4: DNA, GSH (0.513 mM) plus $\mathbf{P^{4+}}$ (0.0128 mM) under aerobic conditions; Lane 5: DNA, GSH (0.513 mM) plus $\mathbf{P^{4+}}$ (0.0128 mM) under anaerobic conditions.

These studies conducted show that $\mathbf{P^{4+}}$ is more effective in bringing about DNA damage under anaerobic conditions as compared to aerobic conditions. To our knowledge, this is the first DNA binding metal-complex to demonstrate potentiated DNA cleavage under hypoxic conditions. We have yet to determine the exact mechanism by which $\mathbf{P^{4+}}$ cuts the DNA. This chapter describes our efforts to further elucidate the mechanism by use of various types of radical scavenging agents. In this manner we aim to establish if the active cleavage agent is a radical species and if so if it is an oxygen or carbon-based radical.

3.2 Results and discussion

3.2.1 DNA cleavage in the presence of oxygen radical scavengers.

Dimethylsulfoxide (DMSO) is known to be an effective scavenger of $^{\bullet}OH$.[53,54]. One simple method to ascertain the presence of oxygen radicals in the DNA cleavage reaction is to add DMSO to the reaction medium in increasing quantities and then to monitor the cleavage activity. DMSO will consume the diffusible oxygen-based radical species and thus we can expect the cleavage activity to by reduced or completely stopped in its presence. The gel shown in Figure 3.4 shows the effect of added DMSO on the cleavage activity of $\mathbf{P}^{4+}$ and GSH, in this case under aerobic conditions. As seen in Lane 4, the combination of $\mathbf{P}^{4+}$ and GSH in air gives a reasonable amount of ss cleavage. Lanes 5, 6 and 7 contain 1%, 3% and 5 % DMSO by volume in the cleavage medium yet show no attenuation of the ss cleavage activity. This result is interpreted as ruling out the role of oxygen radical species in the cleavage mechanism.

For completeness, we repeated the experiment shown in Figure 3.5 under anaerobic conditions. Given the data in Figure 3.4, we do not expect DMSO to have any effect under anaerobic conditions however we know that the active cleaving species is more prevalent under these conditions and thus the reaction was examined. As seen in Figure 3.4, the addition of 1%, 3% and 5 % DMSO in lanes 5, 6 and 7 had no measurable effect of the cleavage activity of the $\mathbf{P}^{4+}$-GSH mixture. It is clear, however, that the overall cleavage activity is better under anaerobic conditions compared to aerobic conditions, as expected.

	1	2	3	4	5	6	7
P^{4+}	-	+	-	+	+	+	+
GSH	-	-	+	+	+	+	+
DMSO	-	-	-	-	1%	3%	5%

Figure 3.4: Agarose gel (1%) stained with ethidium bromide of supercoiled pUC18 DNA (0.154 mM) cleavage products after incubation at 25 ^{o}C for 2 h with P^{4+}, GSH and DMSO in 7 mM Na_3PO_4 buffer (pH 7.0) under aerobic conditions. Lane 1: DNA control ; Lane 2: DNA plus GSH (0.513 mM); Lane 3: DNA plus P^{4+} (0.0128 mM); Lane 4:DNA,GSH (0.513 mM) plus P^{4+}(0.0128 mM); Lane 5: DNA, GSH (0.513 mM), P^{4+}(0.0128 mM) plus 1% DMSO; Lane 6: DNA, GSH (0.513 mM), P^{4+}(0.0128 mM) plus 3% DMSO; Lane 7: DNA, GSH (0.513 mM), P^{4+}(0.0128 mM) plus 5% DMSO.

	1	2	3	4	5	6	7
P^{4+}	-	+	-	+	+	+	+
GSH	-	-	+	+	+	+	+
DMSO	-	-	-	-	1%	3%	5%

Figure 3.5: Agarose gel (1%) stained with ethidium bromide of supercoiled pUC18 DNA (0.154 mM) cleavage products after incubation at 25 ^{o}C for 2 h with P^{4+}, GSH and DMSO in 7 mM Na_3PO_4 buffer (pH 7.0) under anaerobic conditions. Lane 1: DNA control; Lane 2: DNA plus GSH (0.513 mM); Lane 3: DNA plus P^{4+} (0.0128 mM); Lane 4: DNA,GSH (0.513 mM) plus P^{4+}(0.0128 mM); Lane 5: DNA, GSH (0.513 mM), P^{4+}(0.0128 mM) plus 1% DMSO; Lane 6: DNA, GSH (0.513 mM), P^{4+}(0.0128 mM) plus 3% DMSO; Lane 7: DNA, GSH (0.513 mM), P^{4+}(0.0128 mM) plus 5% DMSO.

3.2.2 DNA cleavage in the presence of carbon radical scavengers.

Yamaguchi and coworkers have shown that dihydropyrazines cleave DNA under both aerobic and anaerobic conditions in the presence of trace metals such as Cu^{2+}. While ROS are implicated in the aerobic cleavage chemistry, it is clear that a second cleavage pathway exists which involves carbon radical species and this mechanism is independent of dioxygen.[55-58] As seen in Figure 3.6, complex $\mathbf{P^{4+}}$ contains a similar dihydropyrazine substructure found in many of Yamaguchi's compounds.

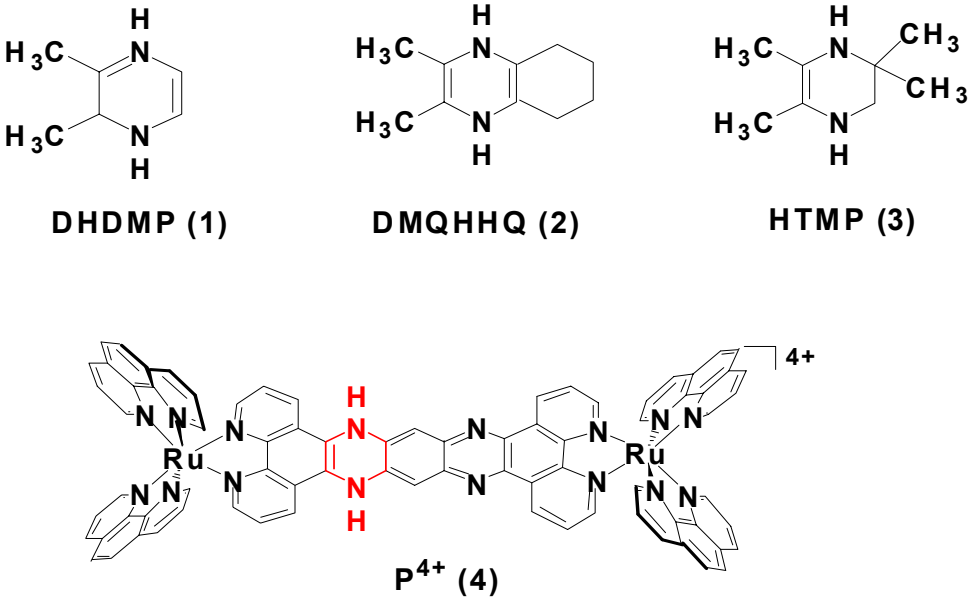

Figure 3.6: **1**, 2,3-Dihydro-5,6-dimethyl-pyrazine(DNDMP); **2**, *trans*-2,3-Dimethyl-5,6,7,8,9,10-hexahydroquinoxaline (DMHHQ); **3**, 3-Hydro-2,2,5,6,-tetramethyl-pyrazine (HTMP); **4**, $\mathbf{P^{4+}}$.

In order to investigate the potential role of carbon radicals in cleavage activity of $\mathbf{P^{4+}}$, we examined the cleavage activity in the presence of 2,2,6,6-tetramethylpipiridine-1-

oxyl (TEMPO), shown in Figure 3.7. TEMPO is a nitroxide species that effectively traps carbon and metal-centered radicals[59,60] by the reaction shown in Figure 3.7.

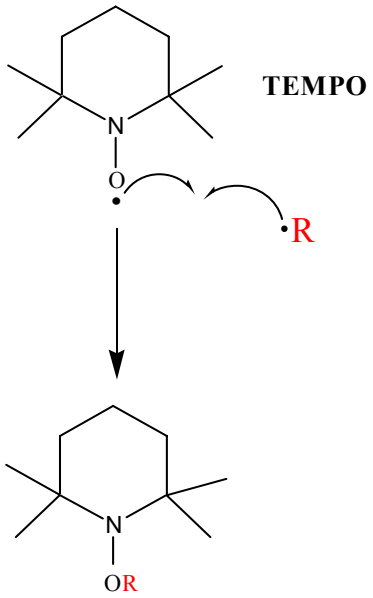

•R Carbon radical

Figure 3.7: Mechanism showing the trapping of carbon based radicals using TEMPO.

As shown in Figure 3.8, the ability of a solution of $\mathbf{P^{4+}}$ and GSH to cleave supercoiled DNA was examined under anaerobic conditions in the presence of increasing amounts of TEMPO. Lanes 3-5 show $\mathbf{P^{4+}}$, GSH and TEMPO at concentrations of 1, 1.5 and 2 mM respectively. As can be seen, the amount of ss cleavage decreases as the TEMPO concentration is increased, suggesting that carbon-centered radicals are involved in the cleavage.

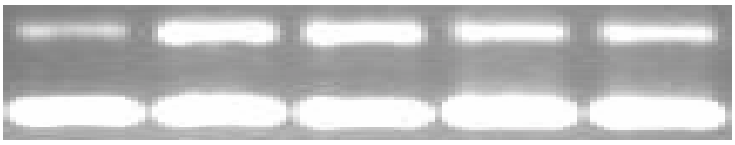

	1	2	3	4	5
P^{4+}	**-**	+	+	+	+
GSH	**-**	+	+	+	+
TEMPO	**-**	**-**	**1**	**1.5**	**2**

Figure 3.8: Agarose gel (1%) stained with ethidium bromide of supercoiled pUC18 DNA (0.154 mM) cleavage products after incubation at 25 ^{o}C for 2 h with $\mathbf{P^{4+}}$ in increasing amounts of TEMPO in 7 mM Na_3PO_4 buffer (pH 7.0) under anaerobic conditions. Lane 1: DNA control; Lane 2: DNA, $\mathbf{P^{4+}}$ (0.0128 mM) plus GSH (0.513 mM); Lane 3: DNA, GSH (0.513 mM), $\mathbf{P^{4+}}$ (0.0128 mM) plus TEMPO (1 mM); Lane 4: DNA, GSH (0.513 mM), $\mathbf{P^{4+}}$ (0.0128 mM) plus TEMPO (1.5 mM); Lane 5: DNA plus GSH (0.513 mM), $\mathbf{P^{4+}}$ (0.0128 mM) plus TEMPO (2.0 mM).

This experiment was repeated with 2 mM TEMPO under both aerobic and anaerobic conditions as shown in Figure 3.9. Under both aerobic and anaerobic conditions, 2 mM TEMPO is sufficient enough to stop most of the cleavage (lanes 6 and 7); however the difference in cleavage yield is most noticeable between anaerobic samples (lane 5 vs. lane 7). This data clearly shows that carbon-based radicals play a role in the cleavage mechanism.

	1	2	3	4	5	6	7
$\mathbf{P^{4+}}$	-	-	+	+	+	+	+
GSH	-	+	-	+	+	+	+
TEMPO	-	-	-	-	-	+	+
$\mathbf{O_2}$	+	+	+	+	-	+	-

Figure 3.9: Agarose gel (1%) stained with ethidium bromide of supercoiled pUC18 DNA (0.154 mM) cleavage products after incubation at 25 ^{o}C for 2 h with $\mathbf{P^{4+}}$, GSH and TEMPO in 7 mM Na_3PO_4 buffer (pH 7.0) under aerobic and anaerobic conditions. Lane 1: DNA control; Lane 2: DNA plus GSH (0.513 mM); Lane 3: DNA plus $\mathbf{P^{4+}}$ (0.0128 mM); Lane 4: DNA, GSH (0.513 mM) plus $\mathbf{P^{4+}}$(0.0128 mM); Lane 5: DNA, GSH (0.513 mM) plus $\mathbf{P^{4+}}$(0.0128 mM) under anaerobic conditions; Lane 6: DNA, GSH (0.513 mM), $\mathbf{P^{4+}}$(0.0128 mM) plus TEMPO (2.04 mM); Lane 7: DNA, $\mathbf{P^{4+}}$(0.0128 mM) plus TEMPO (2.04 mM) under anaerobic conditions .

3.2.3 The effect of Cu^{2+} on DNA cleavage

The TEMPO experiments support the role of carbon radicals in the DNA cleavage mechanism. Yamaguchi and coworkers postulated that Cu^{2+} is needed for the generation of the carbon radical species from the dihydropyrazines in their system. We decided to deliberately add Cu^{2+} to our DNA cleavage medium in order to ascertain the effect of added Cu^{2+} in our system. Figure 3.10 shows the data under both aerobic and anaerobic conditions. Lanes 1 through 4 represent controls. Lane 5 shows that Cu^{2+} (13 μM) alone does not cleave DNA. In the presence of GSH and Cu^{+2} (lane 6), we see some cleavage with ~20% of circular DNA being formed. This is very likely due to the formation of ROS as reduced Cu^{+} reacts with O_2 in solution. A combination of $\mathbf{P^{4+}}$ and

Cu^{2+} (lane 7) also shows some cleavage activity above that of $\mathbf{P^{4+}}$ and DNA alone (lane 3). When GSH, $\mathbf{P^{4+}}$ and Cu^{2+} are combined in the presence of air, we see the complete conversion from supercoiled DNA to circular DNA (lane 8). However, in an oxygen free environment under similar conditions, we observe only ~40% of circular DNA.

	1	2	3	4	5	6	7	8	9
$\mathbf{P^{4+}}$	-	-	+	+	-	-	+	+	+
GSH	-	+	-	+	-	+	-	+	+
$\mathbf{Cu^{+2}}$	-	-	-	-	+	+	+	+	+
$\mathbf{O_2}$	+	+	+	+	+	+	+	+	-

Figure 3.10: Agarose gel (1%) stained with ethidium bromide of supercoiled pUC18 DNA (0.154 mM) cleavage products after incubation at 35 ^{o}C for 2 h with $\mathbf{P^{4+}}$, GSH and Cu^{2+} in 7 mM Na_3PO_4 buffer (pH 7.0). Lane 1: DNA control; Lane 2: DNA plus GSH (0.513 mM); Lane 3: DNA plus $\mathbf{P^{4+}}$ (0.0128 mM); Lane 4: DNA, GSH (0.513 mM) plus $\mathbf{P^{4+}}$(0.0128 mM); Lane 5: DNA plus Cu^{2+} (0.0128 mM); Lane 6: DNA, GSH (0.513 mM) plus Cu^{2+} (0.0128 mM); Lane 7: DNA, $\mathbf{P^{4+}}$(0.0128 mM) plus Cu^{2+} (0.0128 mM); Lane 8: DNA, GSH (0.513 mM), $\mathbf{P^{4+}}$(0.0128 mM) plus Cu^{2+} (0.0128 mM); Lane 9: DNA, GSH (0.513 mM), $\mathbf{P^{4+}}$(0.0128 mM) plus Cu^{2+} (0.0128 mM) under anaerobic conditions.

The dramatic cleavage activity seen in lane 8 shows that all three components can act cooperatively to cause ss cleavage. It is possible that the observed activity is simply the additive effects seen in lanes 4, 6 and 7 but the fact that Cu^{2+} and $\mathbf{P^{4+}}$are interacting to cause cleavage (lane 7) suggests that there may be more involved. The observation that the cleavage activity is at least partially O_2 dependent (compare lanes 8 and 9) clearly suggests a role for ROS generated *via* Fenton-like or Haber-Weiss reactions.

3.2.4 *The role of H_2P^{4+} in DNA cleavage*

The redox chemistry of $\mathbf{P^{4+}}$ in water at pH 7 has been examined and the two reduction products are shown in reaction the reaction below (Figure 3.11).

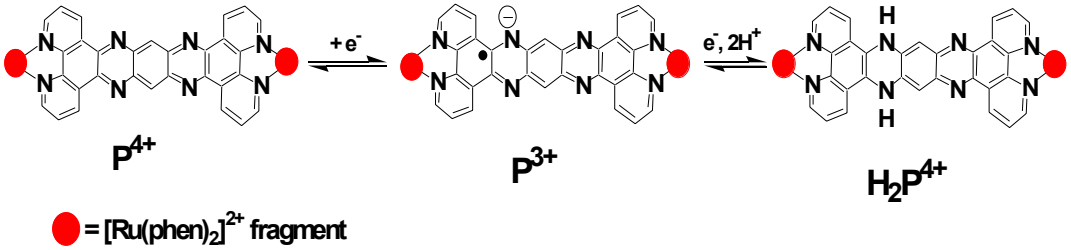

Figure 3.11: Diagram showing the formation of $\mathbf{H_2P^{4+}}$ from $\mathbf{P^{4+}}$.

In order to identify the chemical species responsible for the observed cleavage, the above species were chemically prepared and subjected to agarose gel electrophoresis under anaerobic conditions (Figure 3.12).[50]

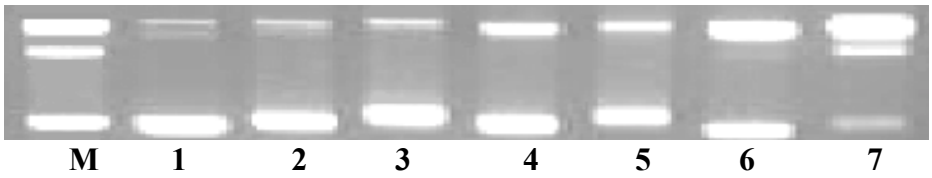

Figure 3.12: Agarose gel (1%) stained with ethidium bromide of supercoiled pUC18 DNA (0.154 mM) cleavage products in the presence of $\mathbf{P^{4+}}$, $\mathbf{P^{3+}}$ and $\mathbf{H_2P^{4+}}$. All incubations were performed under anaerobic conditions with incubation time of 2 h at 25 ^{o}C. Lane M, marker; Lane 1: DNA control; Lane 2: DNA plus $\mathbf{P^{4+}}$ (0.0128 mM); Lane 3: DNA plus $\mathbf{P^{4+}}$ (0.0307 mM), Lane 4: DNA plus $\mathbf{P^{3+}}$ (0.0128 mM); Lane 5: DNA plus $\mathbf{P^{3+}}$ (0.0307 mM), Lane 6: DNA plus $\mathbf{H_2P^{4+}}$ (0.0128 mM); Lane 7: DNA plus $\mathbf{H_2P^{4+}}$ (0.0307 mM).

As seen in lanes 2 and 3, $\mathbf{P^{4+}}$ shows no significant damage to the DNA. The monoreduced complex $\mathbf{P^{3+}}$ shows slightly more cleavage (lanes 4 and 5) than $\mathbf{P^{4+}}$ but only marginally so. Interestingly, the doubly-reduced, doubly-protonated complex

$\mathbf{H_2P^{4+}}$ causes extensive ss cleavage (lanes 6 and 7) with almost full conversion to circular DNA observed with 0.0307 mM $\mathbf{H_2P^{4+}}$ (lane 7). Thus we can assume that the role of GSH in all the prior cleavage assays was to reduce $\mathbf{P^{4+}}$ to $\mathbf{H_2P^{4+}}$ in situ. In fact, we have shown that the absorption spectrum of $\mathbf{P^{4+}}$ in the presence of GSH matches that of $\mathbf{H_2P^{4+}}$. The data shown in Figure 3.13 shows the effect of DMSO and TEMPO on the cleavage activity of $\mathbf{H_2P^{4+}}$ under anaerobic conditions. In addition EDTA was added to one experiment in order to bind any trace metal ions (especially Cu^{2+}) as thus see if trace metals are involved in the cleavage mechanism. The cleavage activity of $\mathbf{H_2P^{4+}}$ was studied in the presence of 5% DMSO, 2 mM TEMPO and 1 mM EDTA which is known to complex trace metals (Figure 3.13).[50]

	M	1	2	3	4	5
$\mathbf{H_2P^{4+}}$		-	+	+	+	+
TEMPO		-	-	-	+	-
DMSO		-	-	+	-	-
EDTA		-	-	-	-	+

Figure 3.13: Agarose gel (1%) stained with ethidium bromide of supercoiled pUC18 DNA (0.154 mM) cleavage products after incubation at 25 ^{o}C for 2 h with $\mathbf{H_2P^{4+}}$ in 7 mM Na_3PO_4 buffer (pH 7.0). Lane 1: Marker lane; Lane 1: DNA control under anaerobic conditions; Lane 2: $\mathbf{H_2P^{4+}}$ (0.0256 mM) plus DNA; Lane 3: DNA, $\mathbf{H_2P^{4+}}$ (0.0256 mM) plus 5% DMSO; Lane 4: DNA, $\mathbf{H_2P^{4+}}$ (0.0256mM) plus TEMPO (1.02 mM); Lane 5: DNA, $\mathbf{H_2P^{4+}}$ (0.0256 mM) plus EDTA (1.02 mM). All reactions were carried out under anaerobic conditions.

Upon the addition of 5% DMSO (lane 3), we see no change in cleavage activity as compared to $\mathbf{H_2P^{4+}}$ alone (lane 2). However, addition of TEMPO stops the cleavage

activity (lane 4). Addition of EDTA had virtually no effect on the cleavage activity, suggesting that trace metal ions are not involved in the observed cleavage activity of $\mathbf{H_2P^{4+}}$. This experiment nicely confirms the prior studies with GSH and supports the hypothesis that carbon-based radicals are playing a role in the DNA cleavage.

3.2.5 Postulated mechanism for DNA cleavage

We know that under anaerobic conditions, $\mathbf{P^{4+}}$ can undergo a one-electron reduction to form $\mathbf{P^{3+}}$. $\mathbf{P^{3+}}$ is a carbon radical-like species and should be capable of extracting H atoms from DNA. However, we observe that pre-prepared solutions of $\mathbf{P^{3+}}$ do not cause significant DNA ss cleavage. We speculate that this is because the radical species $\mathbf{P^{3+}}$ easily dimerizes as shown in Figure 3.14 to form $\mathbf{P_2^{6+}}$. This dimer of dimers would have a difficult time intercalating into the DNA and thus is relatively inactive. Reduction of $\mathbf{P^{4+}}$ by two electrons (plus two protons) forms $\mathbf{H_2P^{4+}}$ which is able to intercalate. Once intercalated into DNA, a one-electron oxidation of $\mathbf{H_2P^{4+}}$ would form a reactive carbon radical species, $\mathbf{P^{3+}}$, that would be unable to dimerize as before and would also be in an optimal position for the radical to attack the DNA duplex. As mentioned earlier, we believe that $\mathbf{P^{3+}}$ is a radical which is capable of abstract hydrogen from the sugar moiety in DNA and hence causing damage.

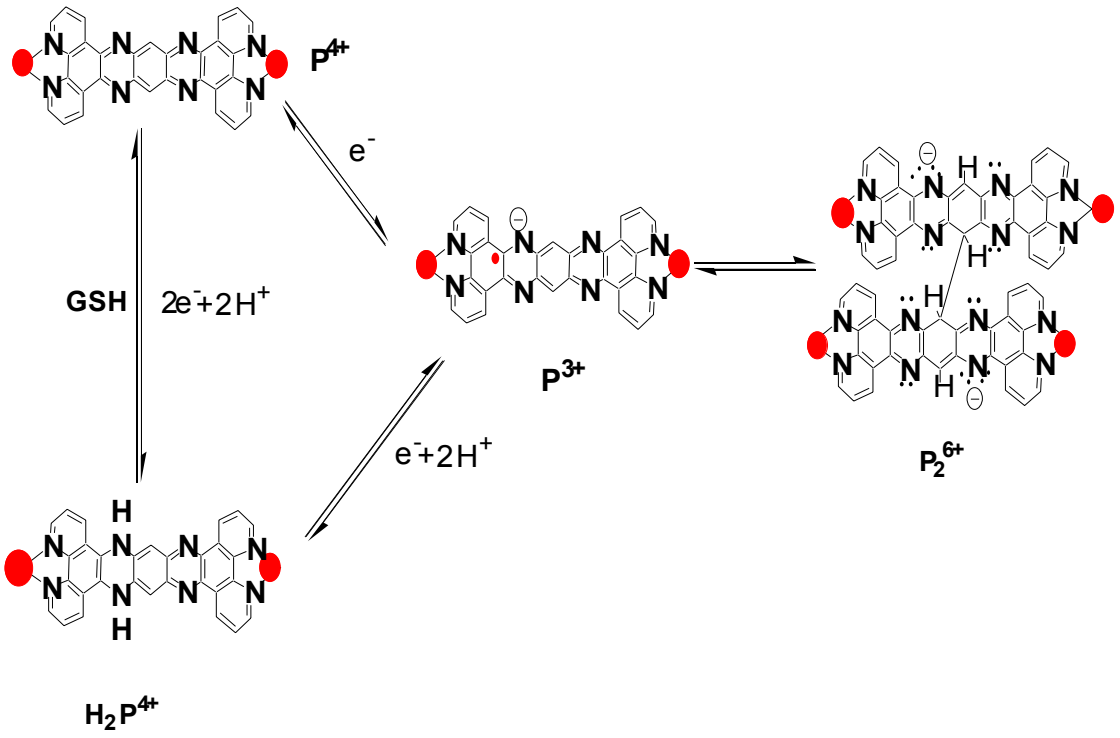

Figure 3.14: Postulated mechanism of DNA cleavage by $\mathbf{P^{3+}}$ species.

At present, we are unable to establish the exact mechanism of DNA cleavage however; we hypothesize that the ultimate active species may be $\mathbf{P^{3+}}$ when it is intercalated into the DNA. We plan on conducting EPR studies to elucidate the cleaving mechanism in the near future.

3.3 Summary and conclusions

We have successfully carried out cleavage studies on $\mathbf{P^{4+}}$ and $\mathbf{H_2P^{4+}}$ using pUC 18 DNA in the presence of different radical scavengers and complexing agents. In the presence of an oxygen radical scavenger (DMSO), we found that there is no effect on DNA cleavage under both aerobic and anaerobic conditions. This proves that ROS do not play a significant role in the DNA mechanism in our system. In the presence of TEMPO, which is a known carbon-centered radical quencher, we see that most of the DNA cleavage stopped both under aerobic and anaerobic conditions. This confirms the role of carbon-based radicals in DNA damage. Cleavage studies of $\mathbf{H_2P^{+4}}$ in the presence of DMSO and TEMPO under aerobic and anaerobic conditions gave similar results as those observed for $\mathbf{P^{4+}}$. We postulate that $\mathbf{H_2P^{+4}}$ is reduced in situ to form $\mathbf{P^{3+}}$ and it is this species that goes on to cleave the DNA through a pathway that has yet to be fully elucidated.

3.4 Experimental

3.4.1 Chemicals

All reagents were purchased commercially and used without further purification unless noted. $[(phen)_2Ru(tatpp)Ru(phen)_2]Cl_4$ ($[\mathbf{P^{4+}}]Cl_4$) was synthesized according to literature methods. Millipore water was used to prepare all buffers. Supercoiled plasmid pUC18 DNA was purchased from Bayou Biolabs (New England). Agarose, ethidium bromide, glutathione (GSH), 2,2,6,6-Tetramethylpiperidine-1-oxyl (TEMPO), Trizma base and $CuSO_4.5H_2O$ were purchased from Sigma Aldrich. DMSO was purchased from Alpha Aesar.

3.4.2 Instrumentation

Plasmid cleavage samples were analyzed using an AlphaImage™ 2200 gel analysis system.

3.4.3 DNA cleavage reactions with DMSO

DNA cleavage reactions with DMSO were carried out in a total volume of 20 µL in 0.5 mL Eppendorf tubes which contained 6 µL of 7 mM Na_3PO_4 buffer medium (pH 7), 4 µL of $\mathbf{P}^{4+}$ (0.0128mM), 4 µL of GSH (1.02 mM), 2 µL of plasmid pUC18 DNA (1 µg/1 µL, 0.154 mM DNA base pairs), and 4 µL of DMSO (1%, 3% or 5% DMSO). The 5% DMSO stock solution was prepared by dissolving 250 µL of DMSO in 750 µL of Millipore water. 1% and 3% solutions were prepared from serial dilutions of the 5 % stock solution. Solutions were left to incubate for 2 h at room temperature and then precipitated by adding 2 µL of 3 M sodium acetate (pH 5.2) and 80 µL of ethanol. The samples were then cooled at -20 ^{o}C overnight. The precipitated DNA was then centrifuged at 13,000 rpm for 30 minutes followed by the removal of the ethanol solution from of the Eppendorfs. The samples were vacuum dried for 30 minutes and then resuspended in 30 µL storage buffer (40 mM Tris-Cl, 1 mM EDTA, pH 8.0) and 10 µL loading buffer (30% glycerol in distilled water with 0.1 % w/v bromophenol blue). After that, 5 µL of each sample was loaded in a 1% agarose gel containing ethidium bromide (0.2 µL/1 mL) and subjected to electrophoresis at 70 V for 2 h using TAE buffer (40 mM Tris-acetate, 1 mM EDTA, pH 8.0). Bands were visualized by UV light and photographed with a UV illuminator.

3.3.4 DNA cleavage reactions with $CuSO_4.5H_2O$

In 0.5 mL Eppendorf tubes, 4 µL $\mathbf{P^{4+}}$ (0.0128 mM) , 4 µL of GSH (1.02 mM), 2 µL of plasmid pUC18 DNA (1 µg/1 µL, 0.154 mM DNA base pairs) and 4 µL of $CuSO_4.5H_2O$ (0.0128 mM) were mixed and made up to a final volume of 20 µL using 7 mM Na_3PO_4 buffer medium (pH 7.0) . The samples were incubated in a 37 ^oC water bath for 2 h and the solutions were subjected to subsequent precipitation and analysis steps similar to those in described 3.6.3.

3.4.5 DNA cleavage reactions with TEMPO

In 0.5 mL Eppendorf tubes, 4 µL P^{4+} (0.0128 mM), 4 µL of GSH (1.02 mM), 2 µL of plasmid pUC18 DNA (1 µg/1 µL, 0.154 mM DNA base pairs), and 4 µL of TEMPO (2 mM) were mixed thoroughly and made up to a final volume of 20 µL using 7 mM Na_3PO_4 buffer medium (pH 7.0), and then left to incubate for 2 h at room temperature. The samples were then subjected to subsequent precipitation and analysis steps similar to those in described 3.6.3.

3.4.6 Synthesis of H_2P^{4+}

$[(phen)_2Ru(tatpp)Ru(phen)_2]Cl_4$ ($[\mathbf{P^{4+}}]Cl_4$) was synthesized according to literature methods. $\mathbf{P^{+4}}$ was placed in the gloved box and 0.1 g was dissolved in 50 mL of degassed Millipore water. In a separate vial, 0.1 g of glutathione was dissolved in 25 mL of degassed Millipore water. The solution of $\mathbf{P^{+4}}$ and GSH were combined and left to stir for 2 h. After 2 h, 0.1 g NH_4PF_6 was added to precipitate the complex. The solution was filtered and the solid was washed with 100 mL of water and 50 mL of ether. The solid was left to stand until it was thoroughly dry. A small amount of the

solid was dissolved in 3 mL degassed acetonitrile and the formation of $[H_2P^{4+}][PF_6]$ was confirmed using UV-Vis spectroscopy. In order to obtain the chloride salt, the solid was dissolved in a minimum volume of acetone and the chloride salt was precipitated with a few drops of tetrabutylammonium chloride in acetone. The solution was filtered and the solid was washed with 25 mL of acetone and left to stand until completely dry. Purity of the product was confirmed using UV-Vis spectroscopy.

3.4.7 DNA cleavage reactions with H_2P^{4+}

All experiment preparation was done in the glove box. In a typical experiment, 5 mg of $\mathbf{H_2P^{4+}}$ was weighed out and dissolved in 1 mL of Millipore water. Of this solution, 20 µL pipetted out and mixed with 980 µL of H_2O to obtain a final concentration of 0.0256 mM. In a 0.5 mL Eppendorf, 4 µL of this solution was added to 2 µL of plasmid pUC18 DNA (1 µg/1 µL, 0.154 mM DNA base pairs) in 7 mM Na_3PO_4 buffer medium (pH 7.0) and left to incubate for 3 h. The solutions were then subjected to subsequent precipitation and analysis steps similar to those in described 3.4.3.

APPENDIX A

ABSORPTION SPECTRA OF $\mathbf{P}^{4+}$ IN THE PRESENCE AND ABSENCE OF DNA, pH 6.0

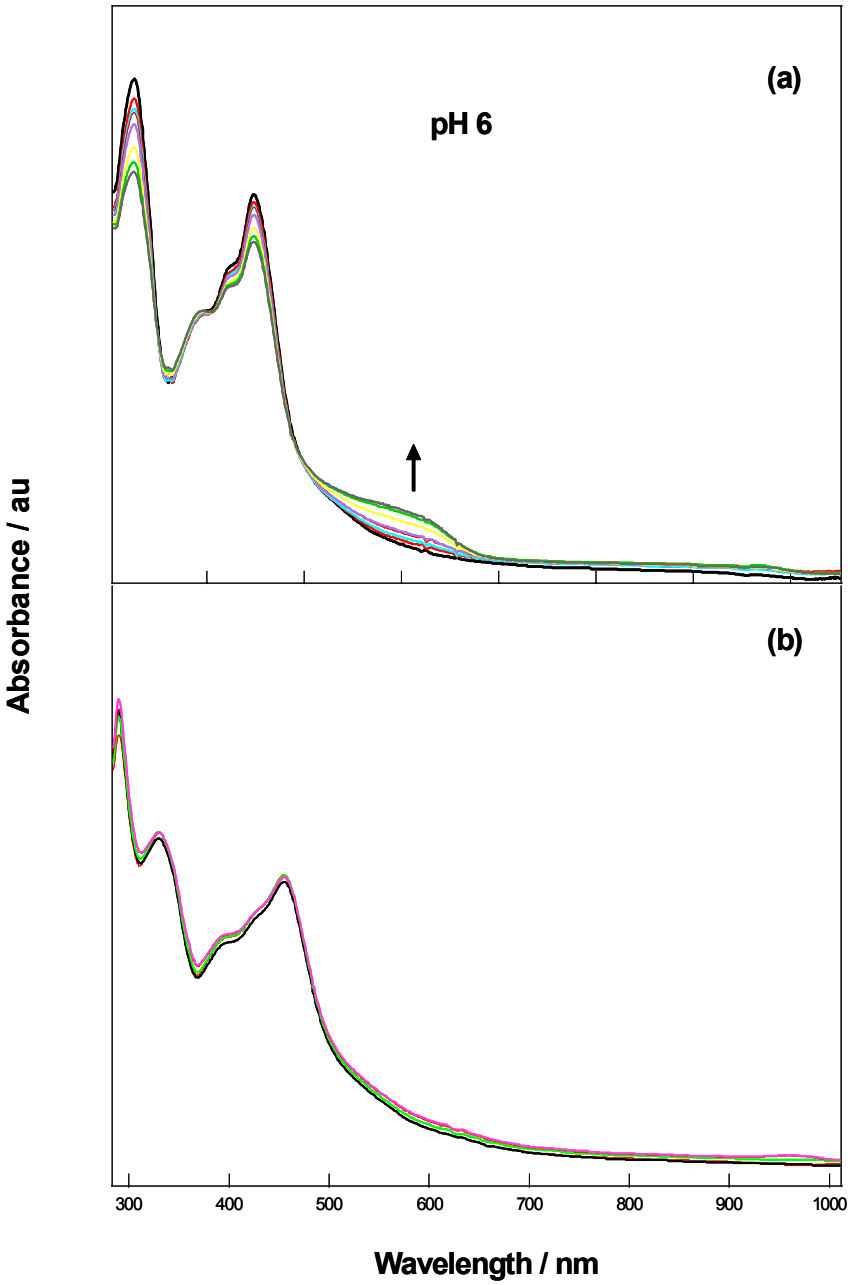

Evolution of absorption spectrum of 16 μM $\mathbf{P}^{4+}$ in 0.1 M TEOA at pH 7.0 (a) In buffer (b) in the presence of DNA ($\mathbf{P}^{4+}$:DNA ratio is 1:12). UV cutoff filter (< 360 nm), distance between light source and sample = 3 cm. Temp 18 ^{o}C.

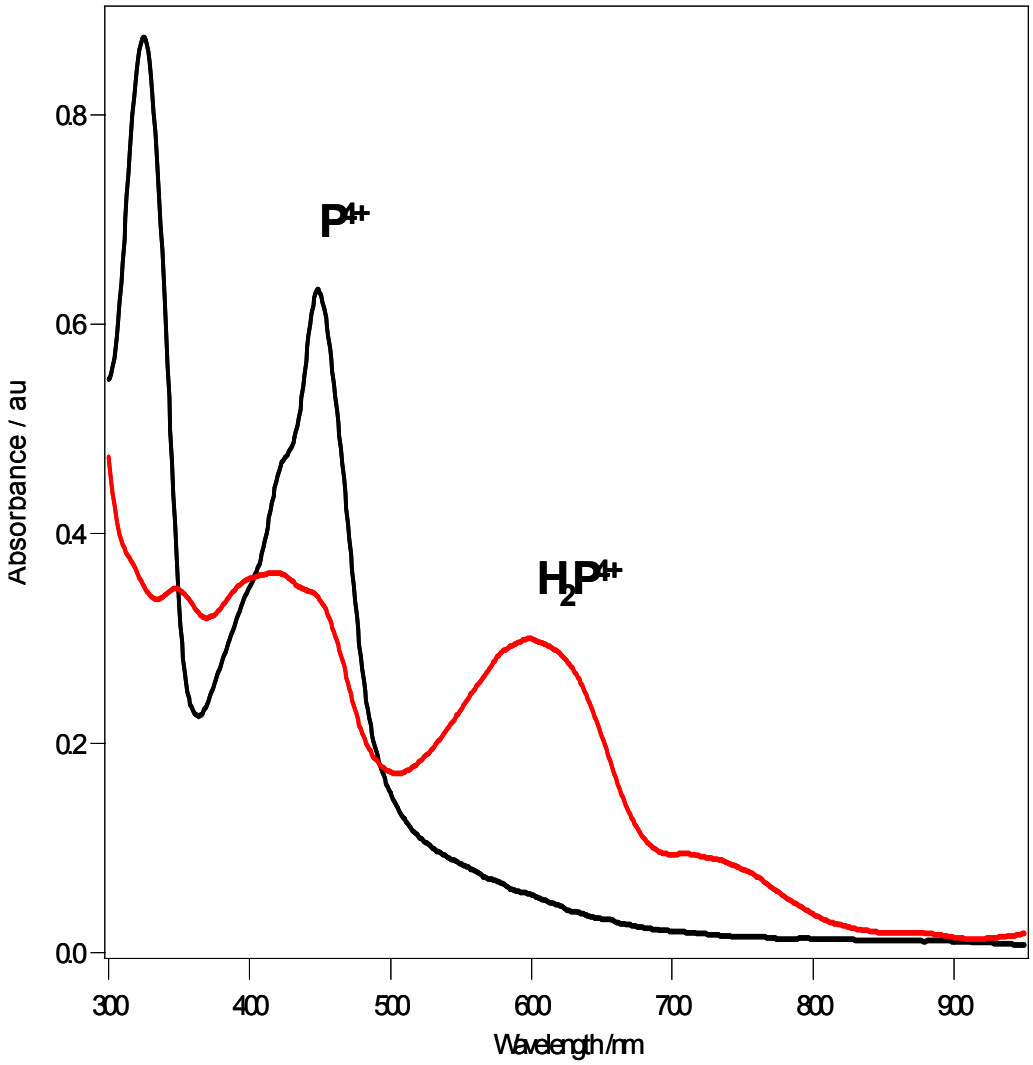

Evolution of absorption spectrum of $\mathbf{H_2P^{4+}}$ and $\mathbf{P^{4+}}$

APPENDIX B

SYNTHESIS OF $\mathbf{P^{4+}}$

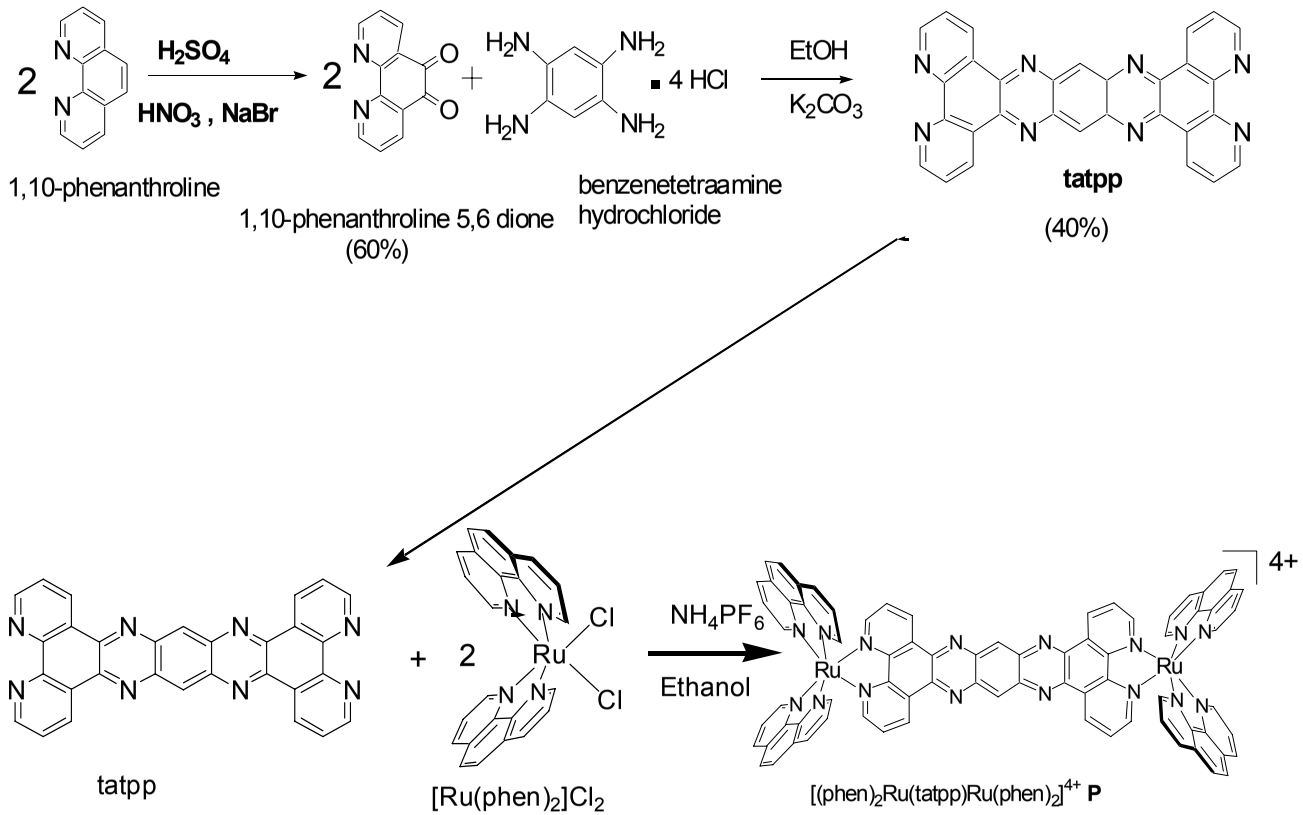
2
H2SO4
HNO3 , NaBr
2
4 HCl
EtOH
K2CO3
1,10-phenanthroline
1,10-phenanthroline 5,6 dione
(60%)
benzenetetraamine
hydrochloride
tatpp
(40%)
tatpp
+ 2
Ru
Cl
Cl
[Ru(phen)2]Cl2
NH4PF6
Ethanol
4+
[(phen)2Ru(tatpp)Ru(phen)2]4+ P

APPENDIX C

^{1}H NMR OF $\mathbf{P^{4+}}$

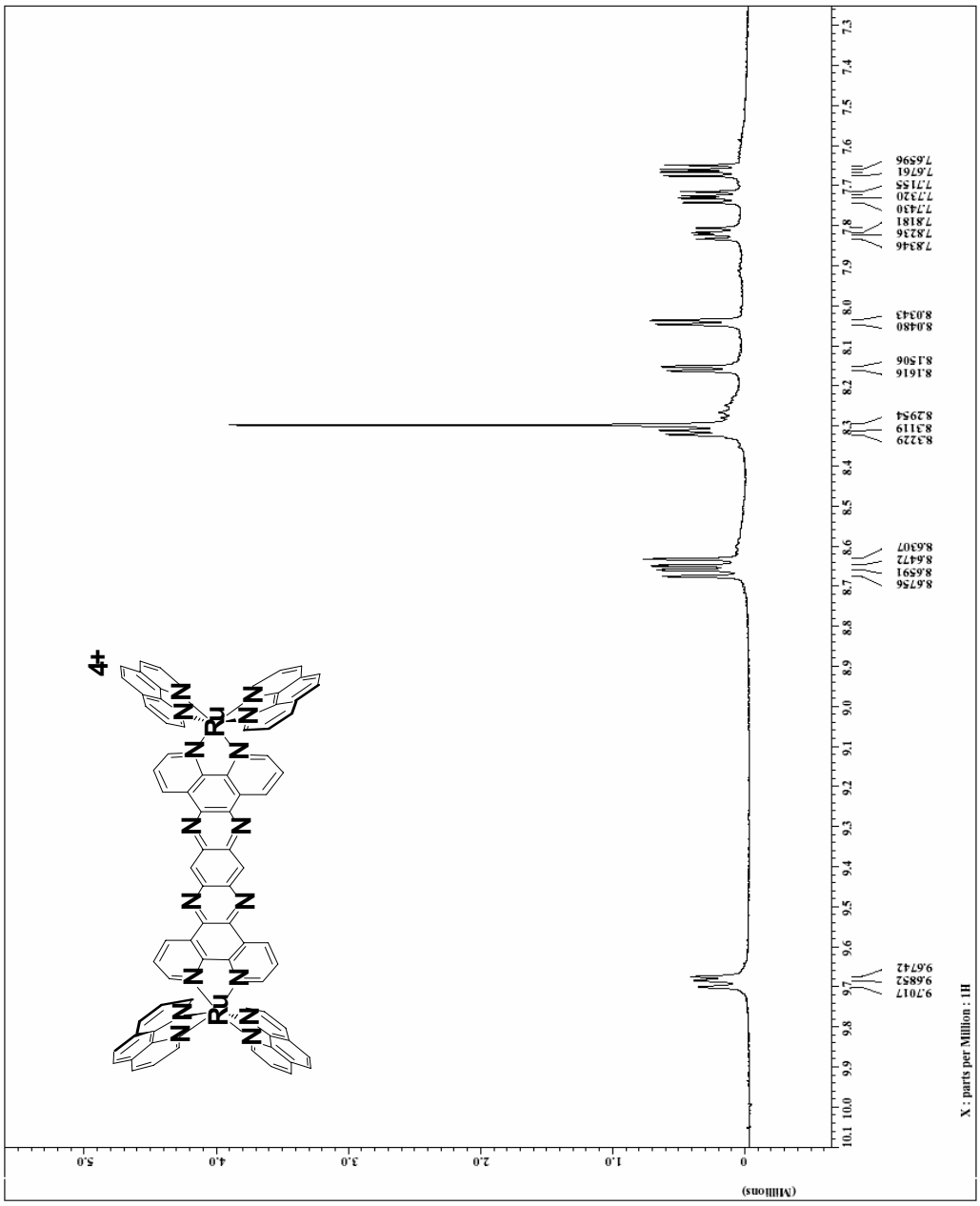
4+
Ru
Ru
N
9.7017
9.6852
9.6742
8.6756
8.6591
8.6472
8.6307
8.3229
8.3119
8.2954
8.1616
8.1506
8.0480
8.0343
7.8346
7.8236
7.8181
7.7430
7.7320
7.7155
7.6761
7.6596
(Millions)
X : parts per Million : 1H

REFERENCES

(1) Rosenberg, B.; Van Camp, L.; Krigas, T. *Science* **1965**, *205*, 698-699.

(2) Abrams, M. J.; Murrer, B. A. *Science* **1993**, *261*, 725-730.

(3) Weiss, R. B.; Christian, M. C. *Drugs* **1993**, *46*, 360-377.

(4) Reedijk, J. *Chem.Commun* **1996**, 801-806.

(5) Wong, E.; Giandomenico, C. M. *Chem.Rev.* **1999**, *99*, 2451-2466.

(6) Blommaert, F. A.; Helma, C. M.; van Dijk-Knijnenburg; Dijt, F. J.; Engelse, L.; Baan, R. A.; Berends, F.; Fichtinger-Schepman, A. J. *Biochemistry* **19995**, *34*, 8474-8480.

(7) Misset, J. L. *Brit.J.Cancer* **1998**, *77*, 4-7.

(8) Uma, V. K.; M.; Weyhermuller, T. N.; U., B. *J.Inorg.Biochem.* **2005**, *99*, 2299-2307.

(9) Barton, J. K.; Erkkila, K. E.; Odom, D. T. *Chem.Rev.* **1999**, *99*, 2777-2796.

(10) Barton, J. K.; Danishefsky, A.; Goldberg.J *J. Am. Chem. Soc* **1984**, *106*, 2172-2176.

(11) Keppler, B. K.; Rupp, W. J.; U. M.; Endres, H.; Niebl, R.; Balzer, W. *Inorg.Chem.* **1987**, *26*, 4366-4370.

(12) Barton, J. K. *J.Biomol.Struct.DynChem.* **1983**, *1*, 621-632.

(13) Satyanarayana, S.; Dabrowiak, J. C.; Chaires; B., J. *Biochemistry* **1992**, *31*, 9319-9324.

(14) Eriksson, M.; Leijon, M.; Hiort, C.; Norden, B.; Graeslund, B. *J. Am. Chem. Soc* **1992**, *114*, 4933-4934.

(15) Friedman, A. E.; Chambron, J. C.; Sauvage, J. P.; Turro, N. J.; Barton, J. K. *J. Am. Chem. Soc* **1990**, *112*, 4960-4962.

(16) Dupureur, C. M.; Barton, J. K. *J. Am. Chem. Soc* **1994**, *116*, 10286-10287.

(17) Dupureur, C. M.; Barton, J. K. *Inorg.Chem* **1997**, *36*, 33-43.

(18) Sava, G.; Bergamo, A. *Int.J.Oncol.* **2000**, *17*, 353-365.

(19) Sava, G.; Pacor, S.; Mestroni, G.; Alessio, E. *Anti-Cancer Drugs* **1992**, 25-31.

(20) Sava, G.; Capozzi, I.; Clerici, K.; Gagliardi, G.; Alessio, E.; Mentroni, G. *Exp.Metastasis* **1998**, *16*, 371-379.

(21) Brown, P. D.; Whittaker, M. *Chem.Rev.* **1999**, *99*, 2735-2776.

(22) Morgunova, E.; Tuutilla, A.; Bergmann, U.; Isupov, M.; Lindqvist, Y.; Schneider, G.; Tryggvason, K. *Science* **1999**, *284*, 1667-1670.

(23) McCord, J. M.; Fridovich, I. *J.Biol.Chem.* **1969**, *244*, 6049-6055.

(24) Heo, J.; Raines, K. W.; Mocanu, V.; Campbell; L., S. *Biochem.* **2006**, *45*, 4481-14489.

(25) Muller, J. G.; Burrows, C. J. *Chem.Rev.* **1998**, *98*, 1109-1151.

(26) Tullius, T. D.; Pogozelski, W. K. *Chem.Rev.* **1998**, *98*, 1089-1107.

(27) Schraufstatter, I.; Hyslop, A. P.; Jackson, H. J.; Cochrane, G. C. *J.Clin.Invest.* **1988**, *82*, 1040-1050.

(28) Floyd, A. R.; Watson, J. J.; Wong, K. P.; Altmiller, H. D.; Rickard, C. R. *Free.Rad.Res.Comm.* **1986**, *137*, 163-172.

(29) Steenken, S. *Chem.Rev.Washington D.C* **1989**, *89*, 503-520.

(30) Cadet, J. B., Maurice *Radiat.Biol.* **1985**, *47*, 127-143.

(31) O'Neill, P. *Radiat.Res.* **1983**, *96*, 198-210.

(32) Kashige, N. Y., Tadatoshi; Miake, Fumio; Watanabe, Kenji *Biol.Phar.Bull.* **2000**, *23*, 1281-1286.

(33) Maeda, M.; Nushi, K. *Tetrahedron* **1974**, *30*, 2677-2682.

(34) Bouskila, A.; Amoulyal, E.; Verchere-Beaur, C.; Sasaki, I.; Gaudmer, A. *Photochem.Photobiol.* **2004**, *76*, 69-83.

(35) Yamagishi, A. *Chem.Commun.* **1983**, *10*, 572-573.

(36) Kim, M.; Konduri, R.; Ye, H.; MacDonnell, F. M.; Puntoriero, F.; Serroni, S.; Campagna, S.; Holder, T.; Kinsel, G.; K.;, R. *Inorg.Chem* **2002**, *41*, 2471-2476.

(37) Kondori, R.; Tacconi, N.; Rajeshwar, K.; MacDonnell, F. M. *J.Am.Chem.Soc.* **2004**, *126*, 11621-11629.

(38) de Tacconi, N. R.; Lezna, R. O.; Konduri, R.; Ongeri, F.; Rajeshwar, K.; MacDonnell, F. M. *Chem.Eur.J.* **2005**, *11*, 4327-4339.

(39) Chiorboli, C.; Fracasso, S.; Scandoloa, F.; Campagna, S.; Serroni, S.; Kondori, R. *Chem.Commun.* **2003**, *14*, 1658-1659.

(40) Kelly.J.M.;; Tossi.A.B.; *Photochem.Photobiol.* **1989**, *49*, 545-556.

(41) Mei, H. Y.; Barton, J. K. *Proc.Natl.Acad.Sci.U.S.A* **1988**, *85*, 1339-1343.

(42) O'Reilly, F.; Kelly, J. M.; Kirsch-DeMesmaeker, A. *Chem.Commun.* **1996**, *9*, 1013-1014.

(43) Barton, J. K. G., Jonathan M.; Kumar, Challa V.; Turro, Nicholas J. *J.Am.Chem.Soc.* **1986**, *108*, 2081-2088.

(44) Janaratne, T. *Doctrate Thesis* **2006**.

(45) Lecomte, J. P.; Kirsch-De Mesmaeker; K.;, A.; M.;, J.; Tossi, A. B.; Gorner, H. *Photochem.Photobiol.* **1992**, *55*, 681-689.

(46) Lecomte, J.; Kirsch-De Mesmaeker; Andree; F; M.;, M.; Kelly, J. M. *Inorg.Chem* **1995**, *34*, 6481-6491.

(47) Keppler, B. K.; Henn, M.; Juhl, U. M.; Berger, M. R.; Niebl, R., ;; Wanger, F. E. *Progress in Clinical Biochemistry and Medicine* **1989**, *10*, 41-69.

(48) Lincoln, P.; Haq, I.; Suh, D.; Norden, B.; Chowdhry, B. Z.; Chaires, J. B. *J.Am.Chem.Soc.* **1995**, *117*, 4788-4796.

(49) Dwyer, F. P.; Gyarfas, E. C.; Rogers, W. P.; Koch, J. H. *Nature* **1952**, *170*, 190-191.

(50) Janaratne, T.; Ongeri, F.; Yadav, A.; MacDonnell, F. M. *Inorg.Chem* **2007**, *In Press*.

(51) Puckett, C. A.; Barton, J. K. *J.Am.Chem.Soc.* **2006**, *129*, 46-47.

(52) Bravo, H. A.; Hernandez, M. E.; Montero, F.; Oliveros, E.; Orellana, G.

J.Phys.Chem.B **2002**, *106*, 4010-4017.

(53) Tu, C.; Shao, Y.; Gan, N.; Xu, Q.; Guo, Z. *Inorg.Chem* **2004**, *43*, 4761-4766.

(54) Ren, R.; Yang, P.; Zheng, W.; Hua, Z. *Inorg.Chem.* **2000**, *39*, 5454.

(55) Yamaguchi, T.; Nomura, H.; Matsunaga, K.; Ito, S.; Takata, J.; Karube, Y. *Biol.Pharm.Bull.* **2003**, *26*, 1523-1527.

(56) Yamaguchi, T.; Matsumoto, S.; Watanabe, K. *Tetrahedron Lett.* **1998**, *39*, 8311-8312.

(57) Yamaguchi, T.; Kashige, N.; Mishiro, N.; Miake, F.; Watanabe, K. *Biol.Pharm.Bull.* **1996**, *19*, 1261-1265.

(58) Yamaguchi, T.; Eto, M.; Harano, K.; Kashige, N.; Watanabe, K.; Ito, S. *Tetrahedron* **1999**, *55*, 675-686.

(59) Connolly, T. J.; Baldový, M. V.; Mohtath, N.; Scaiano, J. C. *Tetrahedron* **1996**, *37*, 4919-4922.

(60) Mohler, D. L.; Downs, J. R.; Hurley-Predecki, A. L.; Sallman, J. R.; Gannett, P. M.; Shi, X. *J.Org.Chem.* **2005**, *70*, 9093-9102.

BIOGRAPHICAL INFORMATION

Fiona Ongeri was born and raised in Kenya. She received her first degree in Pharmaceutical and Chemical Sciences, with Honors from the University of Brighton in 2002. Starting Fall of 2003, she began attending the University of Texas at Arlington for her Masters of Science in Chemistry under the supervision of Professor Frederick M. MacDonnell. Fiona Ongeri graduated from the University of Texas at Arlington in the Spring of 2007.